An Introduction to Dynamical Systems and Neuronal Dynamics

David Terman

January 6, 2004

1 Introduction

A fundamental goal of neuroscience is to understand how the nervous system communicates and processes information. The basic structural unit of the nervous system is the individual neuron which conveys neuronal information through electrical and chemical signals. Patterns of neuronal signals underlie all activities of the brain. These activities include simple motor tasks such as walking and breathing and higher cognitive behaviors such as thinking, feeling and learning [18, 16].

Of course, neuronal systems can be extremely complicated. There are approximately 10^{12} neurons in the human brain. While most neurons consist of dendrites, a soma (or cell body), and an axon, there is an extraordinary diversity of distinct morphological and functional classes of neurons. Moreover, there are about 10^{15} synapses; these are where neurons communicate with one another. Hence, the number of synaptic connections made by a neuron can be very large; a mammalian motor neuron, for example, receives inputs from about 10^4 synapses.

An important goal of mathematical neuroscience is to develop and analyze mathematical models for neuronal activity patterns. The models are used to help understand how the activity patterns are generated and how the patterns change as parameters in the system are modulated. The models can also serve to interpret data, test hypotheses, and suggest new experiments. Since neuronal systems are typically so complicated, one must be careful to model the system at an appropriate level. The model must be complicated enough so that it includes those processes which are believed to play an important role in the generation of a particular activity pattern; however, it cannot be so complicated that it is impossible to analyze, either analytically or computationally.

A neuronal network's population rhythm results from interactions between three separate components: the intrinsic properties of individual neurons, the synaptic properties of coupling between neurons, and the architecture of coupling (i.e., which neurons communicate with each other). These components typically involve numerous parameters and multiple time scales. The synaptic coupling, for example, can be excitatory or inhibitory, and its possible turn on and turn off rates can vary widely. Neuronal systems may include several different types of cells as well as different types of coupling. An important and typically very challenging problem is to determine the role each component plays in shaping the emergent network behavior.

Models for the relevant neuronal networks often exhibit a rich structure of dynamic behavior. The behavior of even a single cell can be quite complicated. An individual cell may, for example, fire repetitive action potentials or bursts of action potentials that are separated by silent phases of near quiescent behavior [27, 15]. Examples of population rhythms include synchronized oscillations, in which every cell in the network fires at the same time and clustering, in which the entire population of cells breaks up into subpopulations or blocks; every cell within a single block fires synchronously and different blocks are desynchronized from each other [10, 31]. Of course, much more complicated population rhythms are possible. The activity may, for example, propagate through the network in a wave-like manner, or exhibit chaotic dynamics [29, 44, 42].

In this article, I will discuss models for neuronal systems and dynamical systems methods for analyzing these models. The discussion will focus primarily on models which include a small parameter and results in which geometric singular perturbation methods have been used to analyze the network behavior. I will not consider other types of models which are commonly used in the study of neural systems. The integrate and fire model of a single cell is one such example. A review of these types of models can be found in [20, 13].

An outline of the article is as follows. Chapters 2 and 3 present an informal introduction to the geometric theory of dynamical systems. I introduce the notions of phase space, local and global bifurcation theory, stability theory, oscillations, and geometric singular perturbation theory. All of these techniques are very important in the analysis of models for neuronal systems. Chapter 4 presents some of the basic biology used in modeling the neuronal systems. I will then discuss the explicit equations for the networks to be considered. Models for single cells are based on the Hodgkin-Huxley formalism [12] and the coupling between cells is meant to model chemical synapses. I will then consider models for single cells that exhibit bursting oscillations.

There are, in fact, several different types of bursting oscillations, and there has been considerable effort in trying to classify the underlying mathematical mechanisms responsible for these oscillations [27, 15]. I then discuss the dynamics of small networks of neurons. Conditions will be given for when these networks exhibit either synchronous or desynchronous rhythms. I conclude by discussing an example of a larger network. This network was introduced as a model for activity patterns in the Basal Ganglia, a part of the brain involved in the generation of movements.

2   One Dimensional Equations

2.1   The Geometric Approach

This chapter and the next provide an informal introduction to the dynamical systems approach for studying nonlinear, ordinary differential equations. A more thorough presentation can be found in [36], for example. This approach associates a picture (the phase space) to each differential equation. Solutions, such as a resting state or oscillations, correspond to geometric objects, such as points or curves, in phase space. Since it is usually impossible to derive an explicit formula for the solution of a nonlinear equation, the phase space provides an extremely useful way for understanding qualitative features of solutions. In fact, even when it is possible to write down a solution in closed form, the geometric phase space approach is often a much easier way to analyze an equation. We illustrate this with the following example.

Consider the first order, nonlinear differential equation

$$\frac{dx}{dt} \;\; = \;\; x - x^3 \;\; \equiv \;\; f(x). \tag{1}$$

Note that it is possible to solve this equation in closed form by separating variables and then integrating. The resulting formula is so complicated, however, that it is difficult to interpret. Suppose, for example, we are given an initial condition, say $x(0) = \pi$, and we asked to determine the behavior of the solution $x(t)$ as $t \to \infty$. The answer to this question is not at all obvious by considering the solution formula.

The geometric approach provides a simple solution to this problem and is illustrated in Fig. 1. We think of $x(t)$ as the position of a particle moving along the x-axis at some time t. The differential equation gives us a formula for the velocity $x'(t)$ of the particle; namely, $x'(t) = f(x)$. Hence, if at time

3

t, $f(x(t)) > 0$, then the position of the particle must increase, while if $f(x(t)) < 0$, then the position must be decrease.

Now consider the solution that begins at $x(0) = \pi$. Since $f(\pi) = \pi - \pi^3 < 0$, the solution initially decreases, moving to the left. It continues to move to the left and eventually approaches the fixed point at $x = 1$. A *fixed point* is a value of x where $f(x) = 0$.

This sort of analysis allows us to understand the behavior of every solution, no matter what its initial position. The differential equation tells us what the velocity of a particle is at each position x. This defines a vector field; each vector points either to the right or to the left depending on whether $f(x)$ is positive or negative (unless x is a fixed point). By following the position of a particle in the direction of the vector field, one can easily determine the behavior of the solution corresponding to that particle.

A fixed point is *stable* if every solution initially close to the fixed point remains close for all positive time. (Here we only give a very informal definition.) The fixed point is *unstable* if it is not stable. In this example, $x = -1$ and $x = 1$ are stable fixed points, while $x = 0$ is unstable.

This analysis carries over for *every* scalar differential equation of the form $x' = f(x)$, no matter how complicated the nonlinear function $f(x)$ is. Solutions can be thought of as particles moving along the real axis depending on the sign of the velocity $f(x)$. Every solution must either approach a fixed point as $t \to \pm\infty$ or become unbounded. It is not hard to realize that a fixed point x_0 is stable if $f'(x_0) < 0$ and is unstable if $f'(x_0) > 0$. If $f'(x_0) = 0$, then one must be careful since x_0 may be stable or unstable.

2.2 Bifurcations

Bifurcation theory is concerned with how solutions of a differential equation depend on a parameter. Imagine, for example, that an experimentalist is able to control the level of applied current injected into a neuron. As the level of applied current increases, the neuron may switch its behavior from a resting state to exhibiting sustained oscillations. Here, the level of applied current represents the bifurcation parameter. Bifurcation theory (together with a good model) can explain how the change in dynamics, from a resting state to oscillations, takes place. It can also be used to predict the value of injected current at which the neuron begins to exhibit oscillations. This may be a useful way to test the model.

There are only four major types of so-called local bifurcations and three of them can be explained using one-dimensional equations. We shall illustrate each of these with a simple example. The fourth major type of local
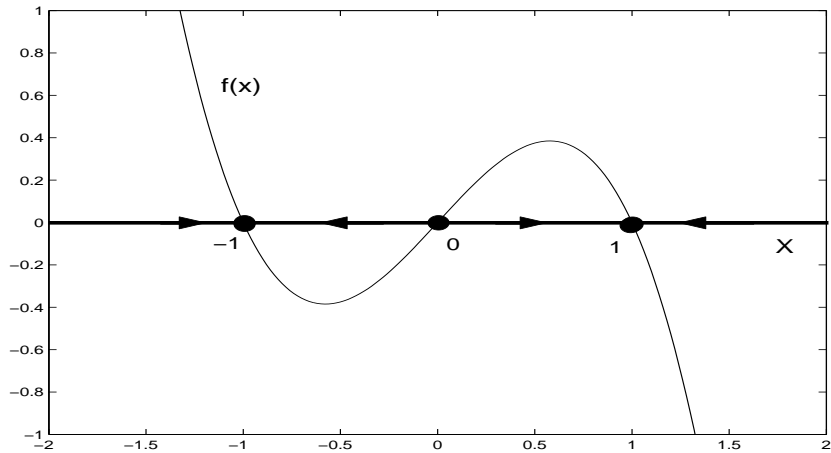
Figure 1: The phase space for Equation (1).

bifurcation is the *Hopf bifurcation*. It describes how stable oscillations arise when a fixed point loses its stability. This requires at least a two dimensional system and is discussed in the next chapter.

Saddle-Node Bifurcation

The following example illustrates the *saddle-node bifurcation*:

$$x' = \lambda + x^2. \tag{2}$$

Here, λ is a fixed (bifurcation) parameter and may be any real number. We wish to solve this equation for a given value of λ and to understand how qualitative features of solutions change as the bifurcation parameter is varied.

Consider, for example, the fixed points of (2) for different values of the bifurcation parameter. Recall that fixed points are those values of x where the right hand side of (2) is zero. If $\lambda < 0$ then (2) has two fixed points; these are at $x = \pm\sqrt{-\lambda}$. If $\lambda = 0$ then there is only one fixed point, at $x = 0$, and if $\lambda > 0$ then there are no fixed points of (2).

To determine the stability of the fixed points, we let $f_\lambda(x) \equiv \lambda + x^2$ denote the right hand side of (2). A fixed point x_0 is stable if $f'_\lambda(x_0) < 0$. Here, differentiation is with respect to x. Since $f'_\lambda(x) = 2x$, it follows that the fixed point at $-\sqrt{-\lambda}$ is stable and the fixed point at $+\sqrt{-\lambda}$ is unstable.

A very useful way to visualize the bifurcation is shown in Fig 2 (left). This is an example of a *bifurcation diagram*. We plot the fixed points $x =$

5

$\pm\sqrt{-\lambda}$ as functions of the bifurcation parameter. The upper half of the fixed point curve is drawn with a dashed line since these points correspond to unstable fixed points, and the lower half is drawn with a solid line since these points correspond to stable fixed points. The point $(\lambda, x) = (0, 0)$ is said to be a *bifurcation point*. At a bifurcation point there is a qualitative change in the nature of the fixed point set as the bifurcation parameter varies.

A basic feature of the saddle-node bifurcation is that as the bifurcation parameter changes, two fixed points, one stable and the other unstable, come together and annihilate each other. A closely related example is $x' = -\lambda + x^2$. There are no fixed points for $\lambda < 0$ and two for $\lambda > 0$. Hence, two fixed points are created as λ increases through the bifurcation point at $\lambda = 0$. This is also referred to as a saddle-node bifurcation.
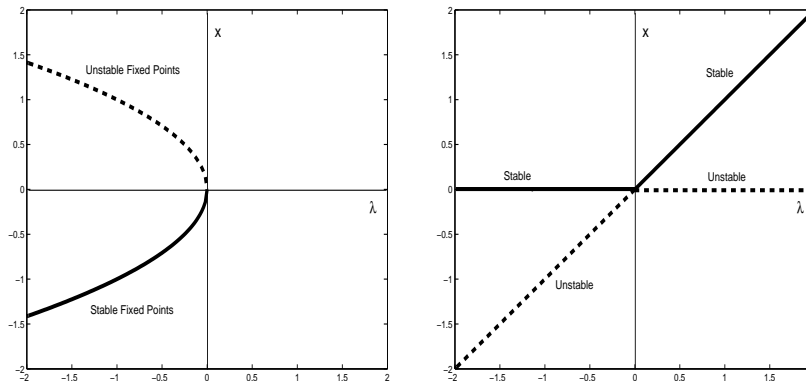

Figure 2: The saddle-node bifurcation (left) and the transcritical bifurcation (right).

Transcritical Bifurcation

A second type of bifurcation is the *transcritical bifurcation*. Consider the equation

$$x' = \lambda x - x^2. \tag{3}$$

Note that $x = 0$ is a fixed point for all values of λ; moreover, there is a second fixed point at $x = \lambda$.

To determine the stability of the fixed points, we let $f_\lambda(x) \equiv \lambda x - x^2$ denote the right hand side of (3). Since $f'_\lambda(x) = \lambda - 2x$, it follows that the fixed point at $x = 0$ is stable if $\lambda < 0$ and is unstable if $\lambda > 0$. The fixed point at $x = \lambda$ is stable if $\lambda > 0$ and is unstable if $\lambda < 0$.

The bifurcation diagram corresponding to this equation is shown in Fig. 2 (right). As before, we plot values of the fixed points versus the bifurcation parameter λ. Solid curves represent stable fixed points, while dashed curves represent unstable fixed points. Note that there is an *exchange of stability* at the bifurcation point $(\lambda, x) = (0, 0)$ where the two curves cross.

Pitchfork Bifurcation

The third type of bifurcation is the *pitchfork bifurcation*. Consider the equation

$$x' = \lambda x - x^3. \tag{4}$$

If $\lambda \leq 0$, then there is one fixed point at $x = 0$. If $\lambda > 0$, then there are three fixed points. One is at $x = 0$ and the other two satisfy $x^2 = \lambda$.

In order to determine the stability of the fixed points, we let $f_\lambda(x) \equiv \lambda x - x^3$. Note that $f'_\lambda(x) = \lambda - 3x^2$. It follows that $x = 0$ is stable for $\lambda < 0$ and unstable for $\lambda > 0$. Moreover, if $\lambda > 0$ then both fixed points $x = \pm\sqrt{\lambda}$ are stable.

The bifurcation diagram corresponding to (4) is illustrated in Fig. 3 (left). There are actually two types of pitchfork bifurcations; (4) is an example of the *supercritical* case. An example of a *subcritical* pitchfork bifurcation is

$$x' = \lambda x + x^3. \tag{5}$$

The bifurcation diagram for this equation is shown in Fig 3 (right). Here, $x_0 = 0$ is a fixed point for all λ. It is stable for $\lambda < 0$ and unstable for $\lambda > 0$. If $\lambda < 0$, then there are two other fixed points; these are at $x_0 = \pm\sqrt{-\lambda}$. Both of these fixed points are unstable.

2.3 Bistability and Hysteresis

Our final example of a scalar ordinary differential equation is:

$$x' = \lambda + 3x - x^3. \tag{6}$$

The bifurcation diagram corresponding to (6) is shown in Fig. 4. The fixed points lie along the cubic $x^3 - 3x - \lambda = 0$. There are three fixed points for $|\lambda| < 2$ and one fixed point for $|\lambda| > 2$. We note that the upper and lower branches of the cubic correspond to stable fixed points, while the middle branch corresponds to unstable fixed points. Hence, if $|\lambda| < 2$ then there are two stable fixed points and (6) is said to be *bistable*.
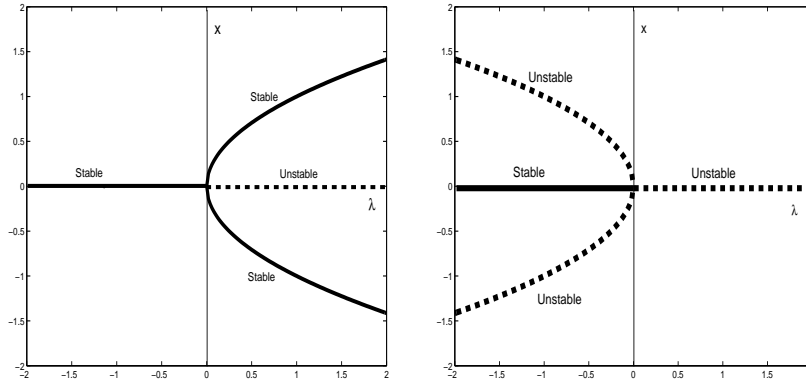
Figure 3: A supercritical pitchfork bifurcation (left) and a subcritical pitchfork bifurcation (right).

There are two bifurcation points. These are at $(\lambda, x) = (-2, 1)$ and $(\lambda, x) = (2, -1)$ and both correspond to saddle-node bifurcations.

Suppose we slowly change the parameter λ, with initially $\lambda = 0$ and x at the stable fixed point $-\sqrt{3}$. As λ increases, (λ, x) remains close to the lower branch of stable fixed points. (See Fig. 4.) This continues until $\lambda = 2$ when (λ, x) crosses the saddle-node bifurcation point at $(\lambda, x) = (2, -1)$. The solution then approaches the stable fixed point along the upper branch. We now decrease λ to its initial value $\lambda = 0$. The solution remains on the upper branch. In particular, $x = \sqrt{3}$ when $\lambda = 0$. Note that while λ has returned to its initial value, the state variable x has not. This is an example of what is often called a *hysteresis phenomenon.*

3   Two Dimensional Systems

3.1   The Phase Plane

We have demonstrated that solutions of first order differential equations can be viewed as particles flowing in a one dimensional phase space. Remarkably, there is a similar geometric interpretation for *every* ordinary differential equation. One can always view solutions as particles flowing in some higher dimensional Euclidean (or phase) space. The dimension of the phase space is closely related to the order of the ode. Trajectories in higher dimensions can be very complicated, much more complicated than the one dimensional examples considered above. In one dimension, solutions (other than fixed points) must always flow monotonically to the left or to the right. In higher
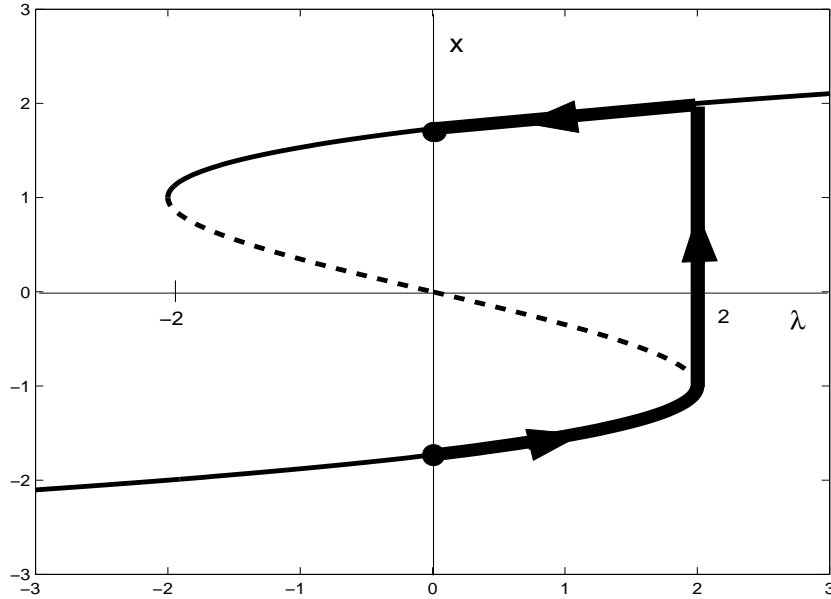
Figure 4: Example of hysteresis.

dimensions, there is a much wider range of possible dynamic behaviors. Here, we consider two dimensional systems, where many of the techniques used to study higher dimensional systems can be introduced.

A two dimensional system is one of the form

$$
\begin{aligned}
x' &= f(x, y) \\
y' &= g(x, y).
\end{aligned}
\tag{7}
$$

Here, f and g are given (smooth) functions; concrete examples are considered shortly. The phase space for this system is simply the $x - y$ plane; this is usually referred to as the *phase plane*. If $(x(t), y(t))$ is a solution of (7), then at each time t_0, $(x(t_0), y(t_0))$ defines a point in the phase plane. The point changes with time, so the entire solution $(x(t), y(t))$ traces out a curve, or trajectory, in the phase plane.

Of course, not every arbitrarily drawn curve in the phase plane corresponds to a solution of (7). What is special about solution curves is that the velocity vector at each point along the curve is given by the right hand side of (7). That is, the velocity vector of the solution curve $(x(t), y(t))$ at a point (x_0, y_0) is given by $(x'(t), y'(t)) = (f(x_0, y_0), g(x_0, y_0))$. This geomet-

9

ric property – that the vector $(f(x,y), g(x,y))$ always points in the direction that the solution is flowing – completely characterizes the solution curves.

3.2 An Example

Consider the system

$$
\begin{aligned}
x' &= y - x^2 + x \\
y' &= x - y.
\end{aligned} \tag{8}
$$

We wish to determine the behavior of the solution that begins at some pre-scribed initial point $(x(0), y(0)) = (x_0, y_0)$. This will be done by analyzing the phase plane associated with the equations.

We begin the phase plane analysis by considering the vector field defined by the right hand side of (8). This is shown in Fig.5 where we have drawn the vector $(y - x^3 + x, x - y)$ at a number of points (x, y). Certainly, one cannot draw the vector field at every point. By considering enough points, one can get a sense of how the vector field behaves, however. A systematic way of doing this is as follows.

The first step is to locate the fixed points. For a general system of the form (7), the fixed points are where both f and g vanish. For the example (8), there are two fixed points; these are at $(0, 0)$ and $(2, 2)$. Later we discuss later how one determines whether a fixed point is stable or unstable.

The next step is to draw the *nullclines*. The *x-nullcline* is where $x' = 0$; this is the curve $y = x^2 - x$. The *y-nullcline* is where $y' = 0$; this is the curve $y = x$. Note that fixed points are where the nullclines intersect. The nullclines divide the phase plane into five separate regions. All of the vectors within a given region point towards the same quadrant. For example, in the region labeled (I), $x' > 0$ and $y' < 0$. Hence, each vector points towards the fourth quadrant as shown. The vector field along the nullclines must be either horizontal or vertical. Along the x-nullcline, the vectors point either up or down, depending on the sign of y'. Along the y-nullcline, the vectors point either to the left or to the right, depending on the sign of x'.

It is now possible to predict the behavior of the solution to (8) with some prescribed initial condition (x_0, y_0). Suppose, for example, that (x_0, y_0) lies in the intersection of the first quadrant with region (I). Since the vector field points towards the fourth quadrant, the solution initially flows with $x(t)$ increasing and $y(t)$ decreasing. There are now three possibilities. The solution must either; (A) enter region II, (B) enter region V, or (C) remain in region I for all $t > 0$. It is not hard to see that in cases A or B, the

10

solution must remain in region II or V, respectively. In each of these three cases, the solution must then approach the fixed point at $(2, 2)$ as $t \to \infty$.
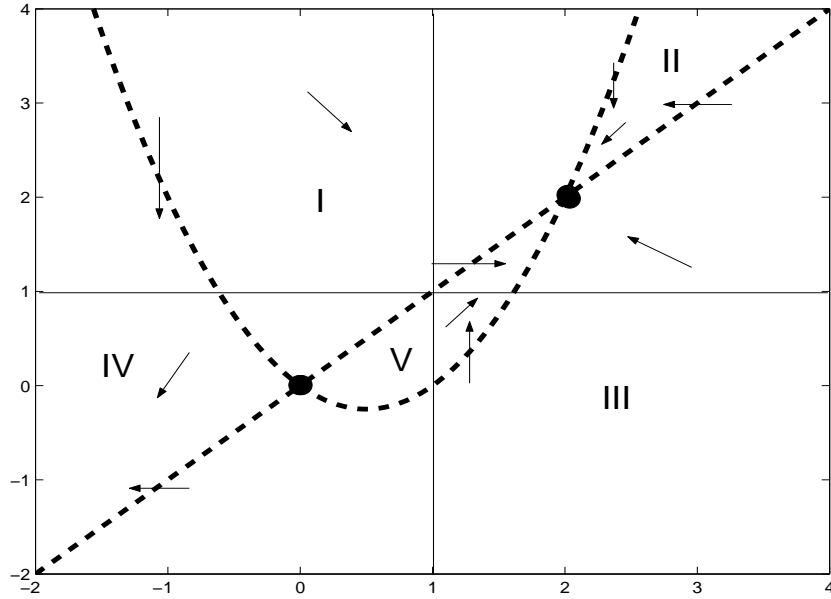

Figure 5: The phase plane for equation (8).

We note that $(0, 0)$ is an unstable fixed point and $(2, 2)$ is stable. This is not hard to see by considering initial data close to these fixed points. For example, every solution that begins in region V must remain in region V and approach the fixed point at $(2, 2)$ as $t \to \infty$. Since one can choose points in region V that are arbitrarily close to $(0, 0)$, it follows that the origin must be unstable.

A more systematic way to determine the stability of the fixed points is to use the method of linearization. This method also allows us to understand the nature of solutions near the fixed point. Here we briefly describe how this important method works; this topic is discussed in more detail in any book on differential equations.

The basic idea of linearization is to replace the nonlinear system (7) by the linear one that best approximates the system near a given fixed point. One can then solve the linear system explicitly to determine the stability of

the fixed point. If (x_0, y_0) is a fixed point of (7), then this linear system is:

$$
\begin{aligned}
x' &= \frac{\partial f}{\partial x}(x_0, y_0)(x - x_0) + \frac{\partial f}{\partial y}(x_0, y_0)(y - y_0) \\
y' &= \frac{\partial g}{\partial x}(x_0, y_0)(x - x_0) + \frac{\partial g}{\partial y}(x_0, y_0)(y - y_0).
\end{aligned}
\tag{9}
$$

Note that the right hand side of (9) represents the linear terms in the Taylor series of $f(x, y)$ and $g(x, y)$ about the fixed point. The stability of the fixed point is determined by the eigenvalues of the Jacobian matrix given by the partial derivatives of f and g with respect to x and y. If both eigenvalues have negative real part, then the fixed point is stable, while if at least one of the eigenvalues has positive real part, then the fixed point must be unstable.

By computing eigenvalues one easily shows that in the example given by (8), $(0, 0)$ is unstable and $(2, 2)$ is stable.

3.3 Oscillations

We say that a solution $(x(t), y(t))$ is *periodic* if $(x(0), y(0)) = (x(T), y(T))$ for some $T > 0$. A periodic solution corresponds to a closed curve or *limit cycle* in the phase plane. Periodic solutions can be either stable or unstable. Roughly speaking, a periodic solution is stable if solutions that begin close to the limit cycle remain close to the limit cycle for all $t > 0$. We do not give a precise definition here.

It is usually much more difficult to locate periodic solutions than it is to locate fixed points. Note that *every* ordinary differential equation can be written in the form $x' = f(x)$, $x \in R^n$ for some $n \geq 1$. A fixed point x_0 satisfies the equation $f(x_0) = 0$ and this last equation can usually be solved with straightforward numerical methods. We also note that a fixed point is a local object – it is simply one point in phase space. Oscillations or limit cycles are global objects; they correspond to an entire curve in phase space that retraces itself. This curve may be quite complicated.

One method for demonstrating the existence of a limit cycle for a two dimensional flow is the Poincare-Bendixson theorem [36]. This theorem does not apply for higher dimensional flows, so we shall not discuss it further. Three more general methods for locating limit cycles are the Hopf bifurcation theorem, global bifurcation theory and singular perturbation theory. These methods are discussed in the following sections.

3.4 Local Bifurcations

Recall that bifurcation theory is concerned with differential equations that depend on a parameter. We saw that one dimensional flows can exhibit saddle-node, transcritical and pitchfork bifurcations. These are all examples of local bifurcations; they describe how the structure of the flow changes near a fixed point as the bifurcation parameter changes. Each of these local bifurcations can arise in higher dimensional flows. In fact, there is only one major new type of bifurcation in dimensions greater than one. This is the so-called Hopf bifurcation. We begin this section by giving a necessary condition for the existence of a local bifurcation point. We then describe the Hopf bifurcation.

We consider systems of the form

$$
\begin{aligned}
x' &= f(x, y, \lambda) \\
y' &= g(x, y, \lambda).
\end{aligned} \tag{10}
$$

It will be convenient to write this system using vector notation. Let

$$
u = (x, y)^T \quad and \quad F(u, \lambda) = (f(x, y, \lambda), g(x, y, \lambda))^T.
$$

Then (10) becomes

$$
u' = F(u, \lambda). \tag{11}
$$

We note that nothing described here depends on (10) being a two dimensional system. The following characterization of a local bifurcation point holds in arbitrary dimensions.

Suppose that u_0 is a fixed point of (10) for some value, say λ_0, of the bifurcation parameter. This simply means that $F(u_0, \lambda_0) = 0$. We will need to consider the Jacobian matrix J of F at u_0. We say that u_0 is a *hyperbolic fixed point* if J does not have any eigenvalues on the imaginary axis. An important result is that if u_0 is hyperbolic, then (u_0, λ_0) cannot be a bifurcation point. That is, a necessary condition for (u_0, λ_0) to be a bifurcation point is that the Jacobian matrix has purely imaginary eigenvalues. Of course, the converse statement may not be true.

We now describe the Hopf bifurcation using an example. Consider the system

$$
\begin{aligned}
x' &= 3x - x^3 - y \\
y' &= x - \lambda.
\end{aligned} \tag{12}
$$

Note that there is only one fixed point for each value of the bifurcation parameter λ. This fixed point is at $(x, y) = (\lambda, \ 3\lambda - \lambda^3)$. It lies along the left or right branch of the cubic x-nullcline if $|\lambda| > 1$ and lies along the middle branch of this cubic if $|\lambda| < 1$.

We linearize (12) about the fixed point and compute the corresponding eigenvalues to find that the fixed point is stable for $|\lambda| > 1$ and unstable for $|\lambda| < 1$. When $|\lambda| = 1$, the fixed points are at the local maximum and local minimum of the cubic; in this case, the eigenvalues are $\pm i$. In particular, the fixed points are not hyperbolic and a bifurcation is possible when $\lambda = \pm 1$.

As λ increases past -1, the fixed point loses its stability. The eigenvalues are complex, so trajectories spiral towards the fixed point for $\lambda < -1$ and trajectories spiral away from the fixed point for $\lambda > -1$. (Here we are assuming that $|\lambda + 1|$ is not too large.) One can show (using a computer) that these unstable trajectories must approach a stable limit cycle. The amplitude of the limit cycle approaches zero as $\lambda \to -1$.

This is an example of a Hopf bifurcation. As the bifurcation parameter varies, a fixed point loses its stability as its corresponding eigenvalues cross the imaginary axis. The Hopf Bifurcation Theorem gives precise conditions for when this guarantees the existence of a branch of periodic orbits.

Note that (12) exhibits two Hopf bifurcations. The first is the one we have just discussed. It takes place when $\lambda = -1$ and the fixed point $(x_0, y_0) = (-1, -2)$ is at the local minimum of the cubic x-nullcline. The second Hopf bifurcation takes place when $\lambda = +1$ and the fixed point $(x_0, y_0) = (1, 2)$ is at the local maximum of the cubic x-nullcline. Figure 6 shows a bifurcation diagram corresponding to (12). Here we plot the maximum value of the x-variable along a solution as a function of the bifurcation parameter λ. The line $x = \lambda$ corresponds to fixed points. This is drawn as a bold, solid line for $|\lambda| > 1$ since these points correspond to stable fixed points, and as a dashed line for $|\lambda| < 1$ since these points correspond to unstable fixed points. There is a curve corresponding to limit cycles that connects the bifurcation points at $(\lambda, x) = (-1, -1)$ and $(1, 1)$.

A Hopf bifurcation may be subcritical or supercritical. In the supercritical case, the limit cycles are stable and they exist for the same parameter values as the unstable fixed points (near the bifurcation point). In the subcritical case, the limit cycles are unstable and exist for those same parameter values as the stable fixed points.
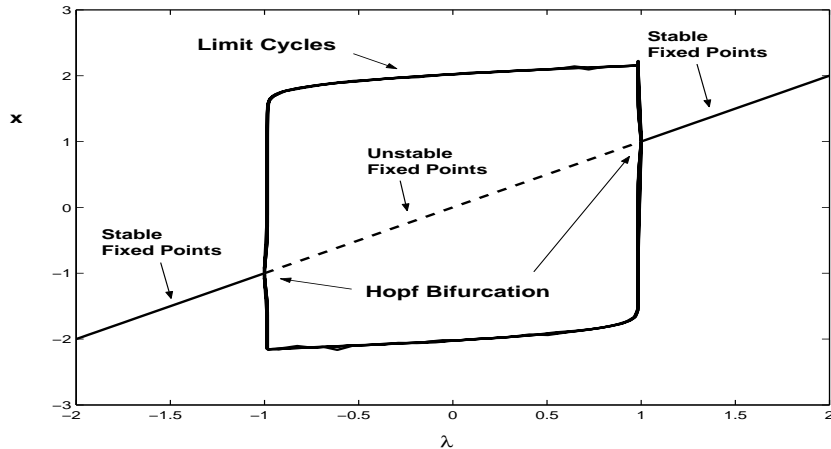
Figure 6: The bifurcation diagram for (12). There are two Hopf bifurcation points.

3.5 Global Bifurcations

Hopf bifurcations are local phenomena; they describe the creation of limit cycles near a fixed point. As the bifurcation parameter approaches some critical value, the limit cycle approaches the fixed point and the amplitude of the limit cycle approaches zero. There are also global mechanisms by which oscillations can be created or destroyed. It is possible, for example, that the amplitude of oscillations remain bounded away from zero, but the frequency of oscillations approaches zero. This will be referred to as a *homoclinic* bifurcation (for reasons described below). It is also possible for two limit cycles, one stable and the other unstable, to approach and annihilate each other at some critical parameter value. This is referred to as a saddle-node bifurcation of limit cycles and resembles the saddle-node bifurcation of fixed points in which two fixed points come together and annihilate each other.

Fig. 7 illustrates a homoclinic bifurcation. For all values of the bifurcation parameter λ there are three fixed points; these are labeled as l, m, and u, and they are stable, a saddle and unstable, respectively. When $\lambda = \lambda_0$ (shown in the middle panel), there is a homoclinic orbit labeled as $\gamma_h(t)$. This orbit lies in both the stable and unstable manifolds of the fixed point m. If $\gamma < \gamma_0$ (shown in the left panel) then there is no periodic orbit, while if $\gamma > \gamma_0$, then there is a stable limit cycle, labeled as $p(t)$. Note that if $\gamma < \gamma_0$, then the stable manifold of m lies inside of the unstable manifold,

15

while the opposite holds if $\gamma > \gamma_0$.

Note that solutions move very slowly as they pass near an unstable fixed point. It follows that the period of the periodic solution, for $\lambda > \lambda_0$, must become arbitrarily large as λ approaches λ_0. We also note that the nature of the three fixed points do not change as λ is varied. Hence, there is no local bifurcation. The homoclinic orbit is a global object, and the limit cycle disappears via a global bifurcation.
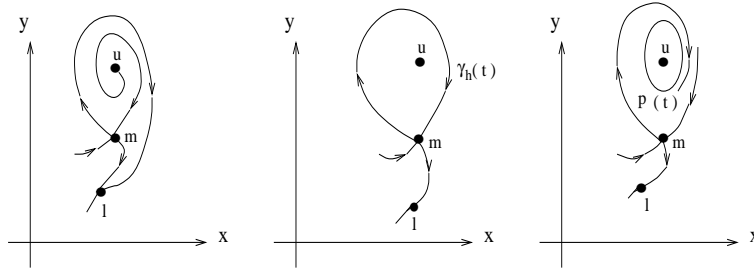

Figure 7: A homoclinic bifurcation.

3.6   Geometric Singular Perturbation Theory

Models for neuronal systems often involve variables that evolve on very different time scales. We shall see many examples of such systems in the next chapter. The existence of different time scales naturally leads to models that contain small parameters. Geometric singular perturbation theory provides a powerful technique for analyzing these models. The theory gives a systematic way to reduce systems with small parameters to lower dimensional reduced systems that are more easily analyzed. Here we illustrate how this method works with a simple example. The method will be used extensively in the next chapter to study more complicated models arising from neuronal systems.

Consider a general two-dimensional system of the form

$$
\begin{aligned}
v' &= f(v, w) \\
w' &= \epsilon g(v, w).
\end{aligned}
\tag{13}
$$

Here, $\epsilon > 0$ is the small, singular perturbation parameter. We assume that the $v-$nullcline is a cubic-shaped curve and the $w-$nullcline is a monotone increasing curve that intersects the cubic at a single fixed point, denoted

16

by p_0, that lies along the middle branch of the cubic nullcline. We also need to assume that $v' > 0 \; (< 0)$ below (above) the cubic $v-$nullcline and $w' > 0 \; (< 0)$ below (above) the $w-$nullcline.

One can prove, using the Poincare-Bendixson theorem, that (13) has a limit cycle for all ϵ sufficiently small. Moreover, the limit cycle approaches a singular limit cycle as shown in Fig. 8 as $\epsilon \to 0$. The singular limit cycle consists of four pieces. One of these pieces lies along the left branch of the cubic nullcline. We shall see in the next chapter that this corresponds to the silent phase of an action potential. Another piece of the singular solution lies along the right branch of the cubic nullcline; this corresponds to the active phase of the action potential. The other two pieces are horizontal curves in the phase plane and they connect the left and right branches. The "jump-up" to the active phase occurs at the left knee of the cubic and the "jump-down" occurs at the right knee of the cubic.

We refer to (13) as a *singular* perturbation problem because the structure of solutions of (13) with $\epsilon > 0$ is very different than the structure of solutions of (13) with $\epsilon = 0$. If we set $\epsilon = 0$, then (13) reduces to

$$
\begin{aligned}
v' &= f(v, w) \\
w' &= 0.
\end{aligned}
\tag{14}
$$

Note that w is constant along every solution of (14); that is, every trajectory is horizontal. The fixed point set is the entire cubic-shaped curve $\{f = 0\}$. This is very different from (13) with $\epsilon > 0$ in which there is only one fixed point and w is not constant along all other solutions.

The reduced system (14) does, however, give a good approximation of solutions away from the cubic $v-$nullcline. In particular, it determines the evolution of the jump-up and jump-down portions of the singular solution. In order to determine the behavior of solutions near the cubic nullcline – that is, during the silent and active phases – we introduce the slow time scale $\tau = \epsilon t$ and then set $\epsilon = 0$ in the resulting system. The leads to the system

$$
\begin{aligned}
0 &= f(v, w) \\
\dot{w} &= g(v, w).
\end{aligned}
\tag{15}
$$

The first equation in (15) implies that the solution of (15) lies along the cubic nullcline. The second equation in (15) determines the evolution of the solution along this nullcline. Note that if we the write the left and right branches of the cubic nullcline as $v = H_L(w)$ and $v = H_R(w)$, respectively,
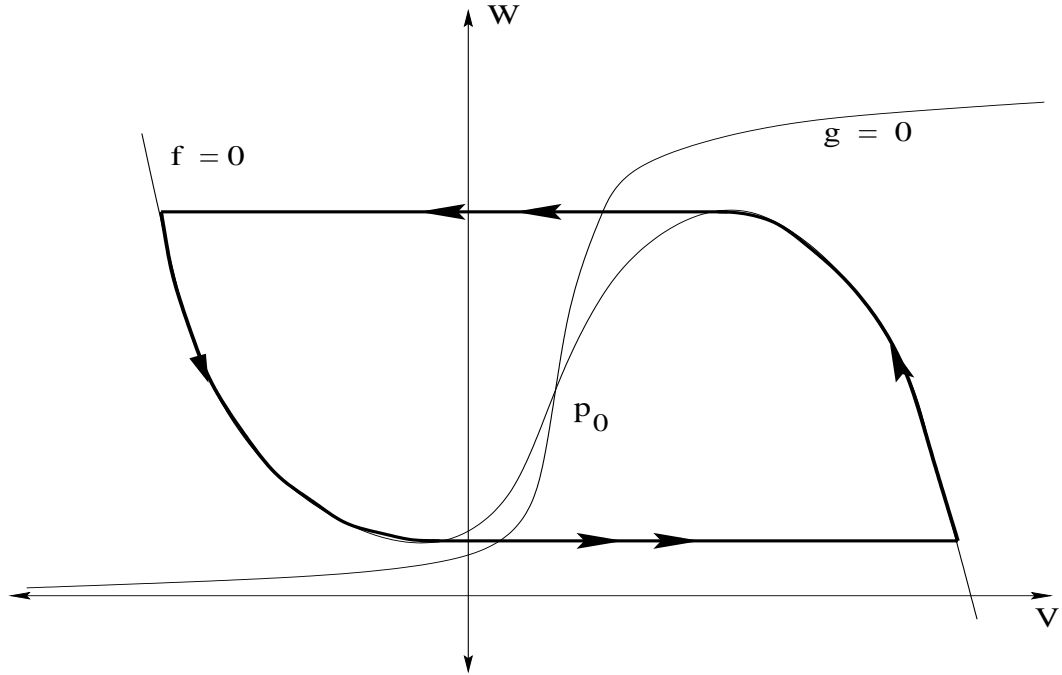
Figure 8: Nullclines and singular periodic orbit for an oscillatory relaxation oscillator.

then we can write the second equation in (15) as

$$\dot{w} \;=\; g(H_\alpha(w), w) \;\equiv\; G_\alpha(w) \tag{16}$$

where $\alpha = L$ or R.

Note that each piece of the singular solution is determined by a single, scalar differential equation. The silent and active phases correspond to solutions of (16). This equation will be referred to as the *slow equation*. The jump-up and jump-down correspond to solutions of the first equation in (14); this is referred to as the *fast equation*.

The analysis described here will be used to study more complicated, higher dimensional systems that arise in models for neuronal systems. Using the existence of small parameters, we will construct singular periodic solutions. Each piece of the singular solution will satisfy a reduced system of equations. We note that the order of the slow equations will be equal to the number of slow variables. In particular, if a given model has one variable that evolves at a much slower time-scale than the other variables,

18

then the order of the slow equations will be just one. Hence, we will reduce the analysis of a complicated, high dimensional system to a single, scalar equation.

4   Single Neurons

In this chapter we discuss models for a single neuron. We begin by quickly reviewing the basic biology that forms the basis of the mathematical models. We then present the Hodgkin-Huxley equations. This is certainly the most important model in computational neuroscience. It was originally introduced as a model for the generation of action potentials in the giant axon of a squid and forms the basis of numerous other models of electrical activity in other neurons. We then present a simpler, reduced model. This will be very useful in our analysis of networks of neuronal activity. We then review geometric analysis of bursting oscillations.

4.1   Some Biology

The neuron is the basic information processing unit in the nervous system. Most neurons consist of a cell body (or soma) and a number of processes that project from the cell body; these are the dendrites and the axon. The dendrites spread out from the cell body in a tree-like manner. They collect incoming signals from other neurons or sensory receptors. Impulses are conducted away from the soma along the axon. Axons may be very short, while others may be very long (up to more than one meter). Many axons develop side branches called axon collaterals that help bring information to several parts of the nervous system simultaneously.

The neuron is surrounded by a cell membrane that maintains a stable resting potential between the outside and the inside of the cell. In response to a stimulus, the membrane potential may undergo a series of rapid changes, called an action potential. This results in the generation of a nerve impulse. In order to form a nerve impulse, the initial stimulus must be above some threshold amount. Properties of the nerve impulse, including its shape and propagation velocity, are often independent of the initial (superthreshold) stimulus.

The resting potential is created because there is an imbalance in the concentrations of certain ions between the inside and the outside of the cell. The intracellular concentrations of sodium and calcium ions are lower than in the extracellular space, while the extracellular potassium concentration is lower than inside the cell. In its resting state, the cell membrane is

permeable to potassium; however it is virtually impermeable to sodium and calcium. The resting potential is about -70 mV and results, to a large extent, from the selective permeability of the membrane and the imbalance in concentration of potassium ions.

Following a stimulus, there is a sudden change in the permeability of the membrane to sodium (or calcium) ions. There are channels in the membrane selective to sodium. An action potential is generated when these channels open and sodium ions rush into the cell interior, causing a rapid rise in the membrane potential. After some delay, the sodium channels close and an increased number of potassium channels open. Potassium ions then flow to the outside of the cell and this brings the membrane towards the resting state. The membrane potential actually overshoots the resting potential. There is a recovery period in which sodium and potassium pumps move sodium and potassium ions, respectively, out of and into the cell until the resting membrane potential is achieved. During the initial phase of this recovery period, it is impossible to generate another action potential. This is referred to as the absolute refractory period.

4.2   The Hodgkin-Huxley Equations

The Hodgkin-Huxley equations were published in 1952 and describe the generation of action potentials in the squid giant axon [12]. The principles underlying the derivation of these equations form the basis of modeling other cells throughout the nervous system. The Hodgkin-Huxley model consists of four differential equations. One of these is a partial differential equation that describes the evolution of the membrane potential. The other three equations are ordinary differential equations that are related to properties of the ionic channels. The Hodgkin-Huxley equations can be written as:

$$
\begin{aligned}
C_M \frac{\partial v}{\partial t} &= D_M \frac{\partial^2 v}{\partial x^2} - g_{Na} m^3 h (v - v_{Na}) - g_K n^4 (v - v_K) - g_L (v - v_L) \\[2mm]
\frac{\partial m}{\partial t} &= (m_\infty(v) - m)/\tau_m(v) \\[2mm]
\frac{\partial n}{\partial t} &= (n_\infty(v) - n)/\tau_n(v) \\[2mm]
\frac{\partial h}{\partial t} &= (h_\infty(v) - h)/\tau_h(v)
\end{aligned}
\tag{17}
$$

Here, $v(x,t)$ represents the membrane potential and each term in the first equation represents a separate current. Since the cell membrane separates charge it can be viewed as a capacitor and $C_M \frac{\partial v}{\partial t}$ is the capacitive current. The term $D_M \frac{\partial^2 v}{\partial x^2}$ represents longitudinal current along the axon and the remaining terms are ionic currents. The sodium current is $I_{Na} \equiv g_{Na} m^3 h (v - v_{Na})$. It is modeled using Ohm's law in which $g_{Na} m^3 h$ is the conductance and $(v - v_{Na})$ is a driving potential. The maximal sodium conductance is g_{Na} and $m^3 h$ can be thought of as the probability that a sodium channel is open. This will be discussed in more detail shortly. The constant v_{Na} is called the *sodium reversal potential*. This is the value of the membrane potential when the sodium concentration, which produces an inward flux of sodium through the sodium channel, is balanced by the electrical potential gradient tending to move sodium ions in the channel in the opposite direction. In a similar manner, $I_K \equiv g_K n^4 (v - v_K)$ is the potassium current with g_K being the maximal potassium conductance and n^4 is the probability that a potassium channel is open. Finally, $I_L \equiv g_L (v - v_L)$ is usually referred to as a leak conductance; it is due to the effects of other, less important, ions including chloride.

Note that the gating variables m, h, and n satisfy differential equations that depend on the membrane potential v. Hence, the probability that a sodium or potassium channel is open or closed depends on the membrane potential. The sodium channel depends on two variables, namely m and h. We can think of the sodium channel as possessing two gates; both gates must be open in order for sodium to flow into the cell. We will not describe the voltage dependent steady-state functions $n_\infty(v), h_\infty(v), n_\infty(v)$ or the time constants $\tau_m(v), \tau_h(v), \tau_n(v)$ here. A detailed description can be found in [16, 19].

What distinguishes one cell from another are the types of ionic currents responsible for the action potential and what factors determine whether the channels corresponding to these ions are open or closed. In what follows, we simplify the presentation by ignoring the spatial dependence of the membrane potential; hence, we only consider systems of ordinary differential equations. Each cell then satisfies a system of the general form

$$
\begin{aligned}
C_M v' &= -I_{ion}(v, w_1, w_2, ..., w_n) + I \\
w_i' &= \epsilon[w_{i,\infty}(v) - w_i]/\tau_i(v).
\end{aligned}
\tag{18}
$$

Here $v(t)$ denotes the membrane potential, I_{ion} is the sum of v- and t-dependent currents through the various ionic channel types and I represents

external applied current. Each variable $w_i(t)$ describes the state of channels of a given type. Each current I_j is assumed to be ohmic and can be expressed as $I_j = \hat{g}_j \sigma_j(v, w_1, ..., w_n)(v - v_j)$ where $\hat{g}_j > 0$, the v_j are constants and the function σ_j represents the fraction of j-channels that are open.

4.3 Reduced Models

The dynamics of even one single neuron can be quite complicated. Examples of such complex behavior are given in the next subsection when we discuss bursting oscillations. We are primarily interested in developing techniques to study networks consisting of possibly a large number of coupled neurons. Clearly the analysis of networks may be extremely challenging if each single element exhibits complicated dynamics. For this reason, we often consider simpler, reduced models for single neurons. The insights we gain from analyzing the reduced models are often extremely useful in studying the behavior of more complicated biophysical models.

An example of a reduced model are the Morris-Lecar equations [24]:

$$
\begin{aligned}
v' &= -g_L(v - v_L) - g_K w(v - v_K) - g_{Ca} m_\infty(v)(v - v_{Ca}) + I \\
w' &= \epsilon(w_\infty(v) - w)\cosh((v + .1)/.3)
\end{aligned}
\tag{19}
$$

The parameters and nonlinear functions in (19) are given by $v_L = -.1$, $g_L = .5$, $g_K = 2$, $v_K = -.7$, $g_{Ca} = 1$, $v_{Ca} = 1$, $\epsilon = .1$, $m_\infty(v) = .5(1 + \tanh((v - .01)/.145))$, $w_\infty(v) = .5(1 + \tanh((v + .1)/.15))$.

These equations can be viewed as a simple model for a neuron in which there are potassium and calcium currents along with the leak current. There is also an applied current represented by the constant I. Here, v represents the membrane potential, rescaled between -1 and 1, and w is activation of the potassium current. Note that the activation of the calcium current is instantaneous. The small, positive parameter ϵ is introduced to emphasize that w evolves on a slow time scale. We treat ϵ as a singular perturbation parameter in the analysis.

Note that this simple model has no spatial dependence; that is, we are viewing the neuron as a single point. This will certainly simplify our analysis of time-dependent oscillatory behavior. In Section 4.5, we add spatial dependence to the model and consider the generation of propagating wave activity.

If $I = 0$, then every solution approaches a stable fixed point. This corresponds to a neuron in its resting state. However, if $I = .4$, then solutions

of (19) quickly approach a stable limit cycle. The periodic solution alternates between an active phase and a silent phase of near resting behavior. Moreover, there are sharp transitions between the silent and active phases.

These solutions can be easily analyzed using the phase space methods described in Section 3.6. The v-nullcline is a cubic-shaped curve, while the w-nullcline is a monotone increasing function that intersects the v-nullcline at precisely one point; hence, there exists precisely one fixed point of (19), denoted by p_0. If $I = 0$, then p_0 lies along the left branch of the cubic v-nullcline and one can easily show that p_0 is asymptotically stable. If, on the other hand, $I = .4$, then p_0 lies along the middle branch of the cubic nullcline and p_0 is unstable. There must then exist a stable limit cycle for all ϵ sufficiently small; moreover, the limit cycle approaches a singular limit cycle as shown in Fig. 8 as $\epsilon \to 0$.

The phase plane analysis does not depend on the precise details of the nonlinear functions and other parameters in (19). We will consider more general two dimensional systems of the form

$$
\begin{aligned}
v' &= f(v, w) + I \\
w' &= \epsilon g(v, w)
\end{aligned}
\tag{20}
$$

where the v-nullcline and the w-nullcline satisfy the assumptions described in Section 3.6.

We note that, with some assumptions, one can systematically reduce a four dimensional Hodgkin-Huxley-like model (without spatial dependence) to a two dimensional Morris-Lecar-like model. One first observes that some of the channel-state variables evolve much faster than others. In particular, the sodium activation variable m evolves on a much faster time-scale than the sodium inactivation variable h and the potassium activation variable n. We therefore assume assume that m activates instantaneously; that is, we set $m = m_\infty(v)$. This reduces the Hodgkin-Huxley equations to just three equations for v, h, n. To reduce the equations further, we observe that along solutions $h \approx \lambda(1 - n)$ for some constant λ. Assuming this to be true, we can eliminate the equation for h and we now have a two-dimensional system similar to the Morris-Lecar equations.

The reduced two-dimensional models given by (19), or more generally (20), exhibit many properties of real neurons. For example, (20) exhibits a refractory period: immediately after an action potential it is difficult to generate another one. This is because when the trajectory in phase space corresponding to the action potential returns to the silent phase, it lies along the left branch of the cubic nullcline with an elevated value of the

recovery variable n. Here, the trajectory is further away from the threshold, corresponding to the middle branch.

Note also that when there is no applied current (that is, $I = 0$), (20) exhibits a stable fixed point; this corresponds to the resting state of a neuron. If I is sufficiently large, then (20) exhibits sustained oscillations. The simple model also displays *excitability*. That is, a small stimulus will not generate an action potential. In this case the solution returns quickly to rest. In order to produce an action potential, the initial stimulus must be larger than some threshold. Note that the threshold corresponds to the position of the middle branch of the cubic nullcline.

Finally, we now discuss how the geometric singular perturbation approach can be used to understand the response of a neuron to injected current. Consider the system

$$
\begin{aligned}
v' &= f(v, w) + I(t) \\
w' &= \epsilon g(v, w)
\end{aligned}
\tag{21}
$$

where f and g are as in (20) and $I(t)$ represents the injected current. We assume that when $I(t) = 0$ the system is excitable; that is, the v- and w-nullclines intersect along the left branch of the cubic. This is a globally stable fixed point and the model neuron is in its resting state. We further assume that there exists I_0 and $T_{on} < T_{off}$ such that

$$I(t) = I_0 \quad \text{if} \quad T_{on} < t < T_{off} \qquad \text{and} \qquad I(t) = 0 \quad \text{otherwise.}$$

We will consider two cases: either $I_0 > 0$, in which case the injected current is said to be *depolarizing*, or $I_0 < 0$ and the injected current is *hyperpolarizing*. Fig. 9 illustrates the neuron's response when (top) $I_0 = .1$ and (bottom) $I_0 = -.1$. In the depolarizing case, the neuron fires an action potential immediately after the injected current is turned on. The cell then returns to rest. In the hyperpolarizing case, the neuron's membrane potential approaches a more negative steady state until the current is turned off, at which time the neuron fires a single action potential. This last response is often called *post-inhibitory rebound* [9].

The geometric approach is very useful in understanding these responses. As before, we construct singular solutions in which ϵ is formally set equal to zero. See Fig. 10. The singular solutions lie on the left or right branch of some cubic-shaped nullcline during the silent and active phases. The cubics depend on the values of $I(t)$. We denote the cubic corresponding to $I = 0$ as C and the cubic corresponding to I_0 as C_0. Note that if $I_0 > 0$, then C_0
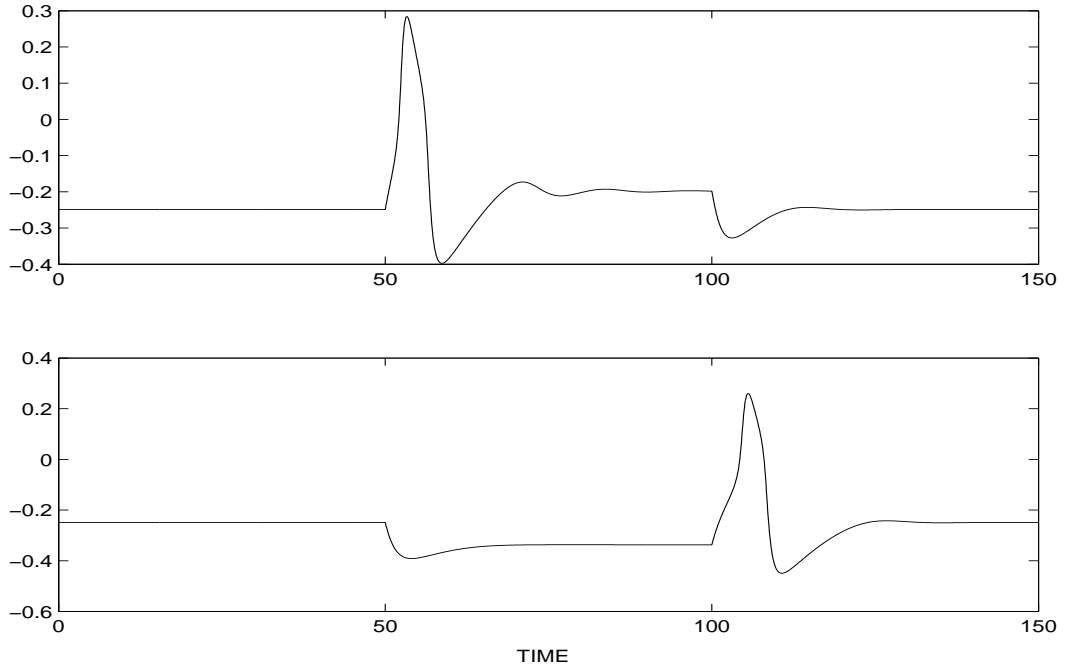
Figure 9: Response of a model neuron to applied current. Current is applied at time $t = 50$ and turned off at $t = 100$. In the top figure, the current is depolarizing ($I_0 = .1$), while in the bottom figure the current is hyperpolarizing ($I_0 = -.1$) and the neuron exhibits post-inhibitory rebound.

lies 'above' C, while if $I_0 < 0$, then C_0 lies 'below' C. This is because of our assumption that $f < 0$ (> 0) above (below) the v-nullcline.

Consider the depolarizing case $I_0 > 0$. This is illustrated in Fig. 10 (left). For $t < T_{on}$, the solution lies at the fixed point p_0 along the left branch of C. When $t = T_{on}$, $I(t)$ jumps to I_0 and the cell's cubic switches to C_0. If the left knee of C_0 lies above p_0 then the cell jumps up to the right branch of C_0; this corresponds to the firing of an action potential. If the w-nullcline intersects C_0 along its left branch, then the cell will approach the stable fixed point along the left branch of C_0 until the input is turned off. It is possible that the w-nullcline intersects C_0 along its middle branch. If this is the case then the cell oscillates, continuing to fire action potentials, until $t = T_{off}$ when the input is turned off. Note that in order for the cell to fire an action potential, the injected current must be sufficiently strong. I_0 must be large enough so that the p_0 lies below the left knee of C_0.

25

Figure 10: Phase space representation of the response of a model neuron to applied current. Current is applied at time $t = T_{on}$ and turned off at $t = T_{off}$. (Left) Depolarizing current. The cell jumps up as soon as the current is turned on. (Right) Hyperplorizing current. The cell jumps to the left branch of C_0 when the current is turned on and jumps up to the active phase due to post-inhibitory rebound when the current is turned off.

We next consider the hyperpolarizing case $I_0 < 0$, shown in Fig. 10 (right). Then C_0 lies below C and the w-nullcline intersects C_0 at a point denoted by p_1. When $t = T_{on}$, the solution jumps to the left branch of C_0 and then evolves along this branch approaching p_1 for $T_{on} < t < T_{off}$. When $t = T_{off}$, I switches back to 0 and the cell now seeks the left or right branch of C. If, at this time, the cell lies below the left knee of C, then the cell will jump up to the active phase giving rise to post-inhibitory rebound. In order to have post-inhibitory rebound, the hyperpolarizing input must be sufficiently large and last sufficiently long. I_0 must be sufficiently negative so that p_1 lies below the left knee of C. Moreover, $T_{off} - T_{on}$ must be sufficiently large so that the cell has enough time to evolve along the left branch of C_0 so that it lies below the left knee of C when the input is turned off.

4.4 Bursting Oscillations

Certain neurons and other excitable cells exhibit bursting oscillations; this behavior is characterized by a silent phase of near steady state resting behavior alternating with an active phase of rapid, spike-like oscillations, as shown in Fig. 11. Examples of biological systems which display bursting oscillations include the Aplysia R-15 neuron, insulin secreting pancreatic beta
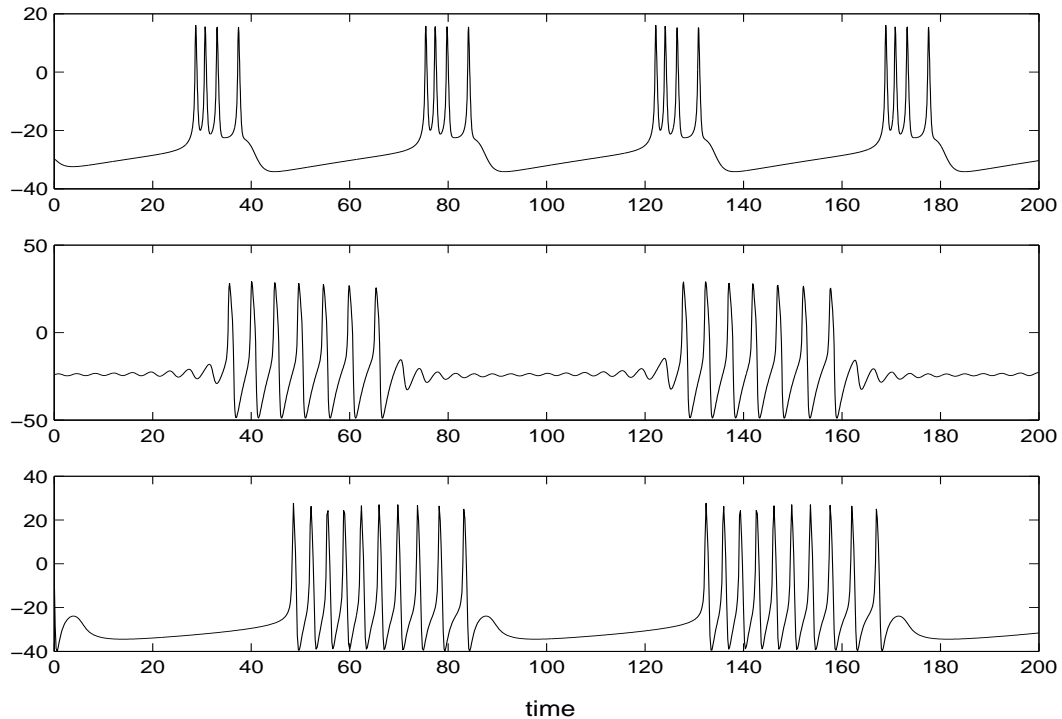
Figure 11: Classes of bursting oscillations. (Top) Square-wave bursting. (Middle) Elliptic bursting. (Bottom) Parabolic bursting.

cells, and neurons in the hippocampus, cortex and thalamus. For references, see [46], for example.

Fig. 11 shows three types of bursting oscillations. Fig. 11 (top) displays an example of *square-wave* bursting. This is characterized by abrupt periodic switching between the quiescent, or silent, phase and the active phase of repetitive firing. Note that the frequency of spikes decreases at the end of the active phase. Fig. 11 (middle) illustrates *elliptic* bursting. Small amplitude oscillations occur during the silent phase and the amplitude of spikes gradually waxes and wanes. Finally, Fig. 11 (bottom) displays *parabolic* bursting. The spike rate first increases and then decreases in a parabolic manner.

The mathematical mechanisms responsible for each class of bursting oscillation are described in terms of geometric properties of the corresponding phase space dynamics. Here we describe the mathematical mechanisms re-

sponsible for square-wave bursting. We only consider the simplest, lowest dimensional, models which generate square-wave bursting. Geometric analysis of other bursting types can be found in [27].

Consider a three-dimensional version of (**??**) of the form

$$
\begin{aligned}
v' &= f(v, w, y) \\
w' &= g(v, w, y) \\
y' &= \epsilon h(v, w, y, \lambda)
\end{aligned}
\tag{22}
$$

Here, $\epsilon > 0$ is a small, singular perturbation parameter and λ is some other fixed parameter. If we set $\epsilon = 0$, then y is constant along solutions and we can think of y as a bifurcation parameter in the fast system (FS) consisting of the first two equations in (22). The primary assumptions on (22) concern the bifurcation structure of the fast subsystem. This structure appears in Fig. 12, which also shows the projection of the square-wave bursting solution onto the corresponding bifurcation diagram. The set of fixed points of (FS) is assumed to be a Z-shaped curve in the (v, w, y) phase space. We denote this curve by S; only a portion of this Z-shaped curve is shown in Fig. 12. The fixed points along the lower branch of S are stable solutions of (FS), while the fixed points on the middle branch of S are saddles. Fixed points along the upper branch of S may be stable or unstable. We also assume that there exists a one-parameter family of periodic solutions of (FS), denoted by P. These limit cycles originate at a Hopf bifurcation along the upper branch of S and terminate along a solution of (FS) that is homoclinic to one of the fixed points on the middle branch of S.

Assumptions are also needed about the slow dynamics. We assume that the y-nullsurface $\{h = 0\}$ defines a two-dimensional manifold that intersects S at a single point. This point lies on the middle branch of S between the homoclinic point and the right knee of S. Finally, $h > 0$ above $\{h = 0\}$ and $h < 0$ below $\{h = 0\}$.

We now give a heuristic explanation for why this system generates a square-wave bursting solution. Suppose that $\epsilon > 0$ is small and consider a solution that begins close to the lower branch. Because this branch consists of stable fixed points of (FS), the trajectory quickly approaches a small neighborhood of the lower branch. The trajectory tracks rightward along the lower branch according to the slow dynamics, until it passes the right knee. This portion of the solution corresponds to the silent phase. Once past the right knee, the trajectory is attracted to near P, the branch of periodic solutions of (FS). This generates the fast repetitive spikes of the bursting solutions. The trajectory passes near P, with decreasing y, until
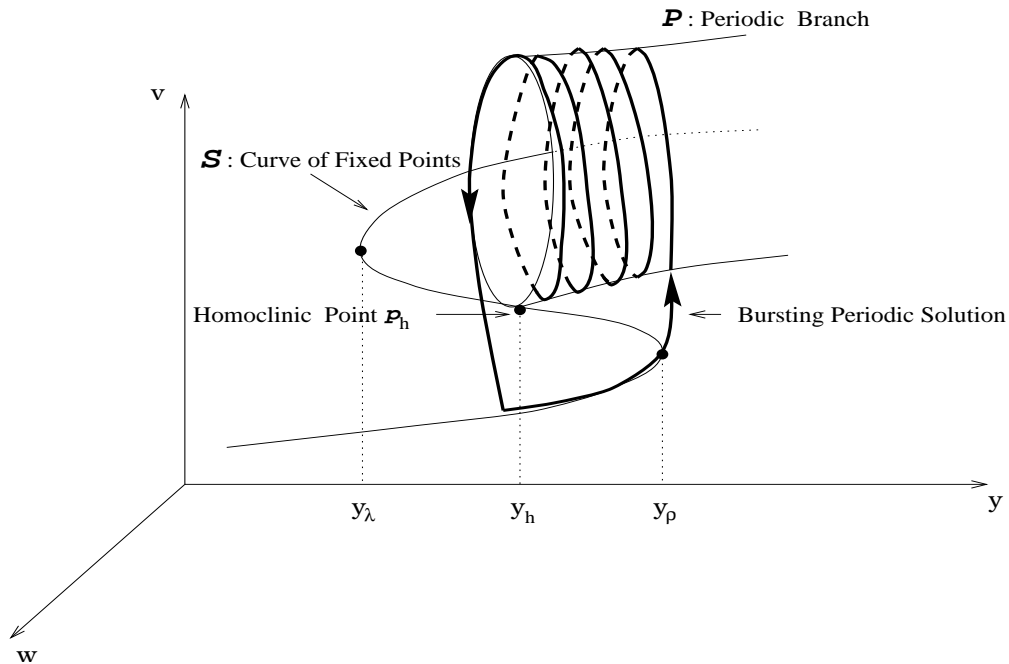
Figure 12: Bifurcation structure for square-wave bursting. The bold curve is the projection of a square-wave bursting solution.

it reaches a neighborhood of the homoclinic orbit of (FS). Once it passes the homoclinic orbit, the fast dynamics eventually forces the trajectory back to near the lower branch of S and this completes one cycle of the bursting solution.

This description is formal. It is not at all clear that if the system (22) satisfies the above assumptions, then, for all ϵ sufficiently small, there exists a unique periodic solution corresponding to a bursting oscillation. In fact, it is shown in [38] that such a result cannot be true, in general. However, in [22], it is proved that the bursting solution will be uniquely determined for all ϵ sufficiently small, except for those ϵ that lie in a certain very small set.

Remark 4.1 A crucial ingredient for square-wave bursting is bistability. This allows for a hysteresis loop between a lower branch of stable fixed points and an upper branch of stable limit cycles. It is also very important that the slow nullsurface $\{h = 0\}$ lies between these two branches. If this

last condition is not satisfied, then the system may exhibit other types of solutions. For example, suppose that $\{h = 0\}$ intersects the lower branch of S. This point of intersection will then be a globally stable fixed point of (22). If, on the other hand, $\{h = 0\}$ intersects S along its middle branch above the homoclinic point, then (22) may give rise to a stable limit cycle which always remains in the active phase near P. This type of solution is referred to as *continuous spiking*. Rigorous results concerning the existence of continuous spiking are presented in [39].

Remark 4.2 Square-wave bursting arises in models for electrical activity in pancreatic β-cells. It is believed that this activity plays an important role in the release of insulin from the cells. The first mathematical model for this bursting was due to Chay and Keizer [5]. There have been numerous related models, based on experimental data, since then. A review of these models, along with a detailed description of the more biological issues, is given in [32]. Square wave bursting also arises in recent models for respiratory CPG neurons [3] and models for pattern generation based on synaptic depression [37].

Remark 4.3 Very complicated (global) bifurcations can take place as the parameters ϵ or λ are varied in (22). The singular perturbation parameter ϵ controls the rate at which a bursting trajectory passes through the silent and active phases. In particular, the number of spikes per burst is $O(1/\epsilon)$ and becomes unbounded as $\epsilon \to 0$. It is demonstrated in [38] that Smale horseshoe chaotic dynamics can arise during the transition of adding a spike.

Perhaps even more interesting is the bifurcation structure of (22) as λ is varied. In the β-cell models, λ is related to the glucose concentration. As the glucose level gradually increases, the cells exhibit resting behavior, then bursting oscillations, and then continuous spiking. This is consistent with behavior exhibited by the model. As λ increases, the y-nullsurface $\{h = 0\}$ intersects the lower branch of S, then the middle branch of S below the homoclinic point, and then the middle branch of S above the homoclinic point. Numerical studies [6] and rigorous analysis [39] have shown that as λ varies between the bursting and continuous spiking regimes, the bifurcation structure of solutions must be very complicated. A Poincaré return map defined by the flow from a section transverse to the homoclinic orbit of (FS) will exhibit Smale-horseshoe dynamics for a robust range of parameter values. This leads to solutions in which the number of spikes per burst varies considerably.

Remark 4.4 Some phenomenological, polynomial models for square-wave bursting have been proposed. See, for example, [11], [25], [7]. Analysis of models with two slow variables which exhibit square-wave bursting is given in [33].

Remark 4.5 A system of equations which give rise to square-wave bursting is [28]:

$$
\begin{aligned}
v' &= -(g_{ca}m_\infty(v)(v - v_{ca}) + g_k w(v - v_k) + g_l(v - v_l) + g_{kca}z(y)(v - v_k)) + I \\
w' &= 20\phi(w_\infty(v) - w)/\tau(v) \\
y' &= 20\epsilon(-\mu g_{ca}m_\infty(v)(v - v_{ca}) - y)
\end{aligned}
$$

where, $g_{ca} = 4.$, $g_k = 8.0$, $g_l = 2.0$, $v_k = -84$, $v_l = -60$, $v_{ca} = 120.0$, $I = 45$, $g_{kca} = .25$, $\phi = .23$, $\epsilon = .005$, and $\mu = .02$. The nonlinear functions are given by $m_\infty(v) = .5(1. + \tanh((v + 1.2)/18))$, $w_\infty(v) = .5(1. + \tanh((v - 12)/17.4))$, $z(y) = y/(1 + y)$ and $\tau(v) = \cosh((v - 12.)/34.8)$.

4.5 Traveling Wave Solutions

We have so far considered a model for neurons that ignores the spatial dependence. This has allowed us to study how temporal oscillatory behavior arises. One of the most important features of neurons is the propagating nerve impulse and this clearly requires consideration of spatial dynamics. The nerve impulse corresponds to a traveling wave solution and there has been extensive research on the mathematical mechanisms responsible for both the existence and stability of these types of solutions. Here we briefly illustrate how one constructs a traveling wave solution in a simple model, the FitzHugh-Nagumo equations. References related to this important topic are given later.

The FitzHugh-Nagumo equations can be written as:

$$
\begin{aligned}
v_t &= v_{xx} + f(v) - w \\
w_t &= \epsilon(v - \gamma w).
\end{aligned}
\tag{23}
$$

Here, (v, w) are functions of $(x, t), x \in R$ and $t \geq 0$. Moreover, $f(v) = v(1 - v)(v - a)$, $0 < a < 1/2$, ϵ is a small singular perturbation parameter, and γ is a positive constant chosen so that the curves $w = f(v)$ and $v = \gamma w$ intersect only at the origin.

A traveling wave solution of (23) is a solution of the form $(v(x, t), w(x, t)) = (V(z), W(z)), z = x + ct$; that is, a traveling wave solution corresponds to a

solution that propagates with constant shape and velocity. The velocity is c as in not known a priori. We also assume that the traveling wave solution satisfies the boundary conditions $\lim_{z \to \pm\infty}(V(z), W(z)) = (0, 0)$.

Note that a traveling wave solution corresponds to a solution of the first order system of ordinary differential equations

$$
\begin{aligned}
V' &= Y \\
Y' &= cY - f(V) + W \\
W' &= \frac{\epsilon}{c}(V - \gamma W)
\end{aligned}
\tag{24}
$$

together with the boundary conditions

$$
\lim_{z \to \pm\infty}(V(z), Y(z), W(z)) = (0, 0, 0)
\tag{25}
$$

Hence, a traveling wave solution corresponds to a homoclinic orbit of a first order system. This homoclinic orbit will exist only for special values of the velocity parameter c.

One can use geometric singular perturbation methods, as described in Section 3.6, to construct a singular homoclinic orbit in which ϵ is formally set equal to zero. One needs to then rigorously prove that this singular solution perturbs to an actual homoclinic orbit that lies near the singular orbit for ϵ sufficiently small.

The singular orbit is constructed as follows. As before, the singular orbit consists of four pieces, as shown in Fig. 13. Two of these pieces correspond to the silent and active phases and the other two pieces correspond to the jump-up and jump-down between these phases. As before, we consider both fast and slow time scales.

The jump-up and jump-down pieces correspond to solutions of the fast equations. These are obtained by simply setting $\epsilon = 0$ in (24). The resulting equations are:

$$
\begin{aligned}
V' &= Y \\
Y' &= cY - f(V) + W \\
W' &= 0
\end{aligned}
\tag{26}
$$

Note that W must be constant along this solution. For the jump-up (or front), we set $W \equiv 0$ and look for a solution of the first two equations of (24) that satisfy

$$
\lim_{z \to -\infty}(V, Y) = (0, 0) \quad \lim_{z \to +\infty}(V, Y) = (1, 0)
\tag{27}
$$

It is well known that there exists a unique solution for a unique value of the parameter c. We denote this parameter as c_0. This is the velocity of the wave in the limit $\epsilon \to 0$.

For the jump-down (or back) we set $W \equiv W_0$, where W_0 is chosen so that if $c = c_0$ then there exists a solution of the first two equations in (26) such that $\lim_{z \to -\infty}(V, Y, W_0)$ lies along the right branch of the cubic $W = f(V)$ and $\lim_{z \to +\infty}(V, Y, W_0)$ lies along the left branch of this cubic. This is shown in Fig. 13. We note that W_0 is indeed uniquely determined.

We now consider the pieces of the singular traveling wave solution corresponding to the silent and active phases. We introduce the slow time scale $\eta = \epsilon z$ and then set $\epsilon = 0$ to obtain the slow equations

$$
\begin{aligned}
Y &= 0 \\
W &= f(V) \\
\dot{W} &= \frac{1}{c_0}(V - \gamma W)
\end{aligned}
\tag{28}
$$

Here $\dot{W}$ corresponds to differentiation with respect to η. These equations demonstrate that during the silent and active phases, the singular solution lies along the cubic curve defined by $W = f(V)$, $Y = 0$. The complete singular homoclinic orbit is shown in Fig. 13.

Remark 4.6 References to rigorous studies of the existence and stability of traveling wave solutions can be found in [17].

5 Two Mutually Coupled Cells

5.1 Introduction

In this section, we consider a network consisting simply of two mutually coupled cells. By considering such a simple system, we are able to describe how we model networks of oscillators, the types of behavior that can arise in such systems and the mathematical techniques we use for the analysis of the behavior. For this discussion, we assume that each cell, without any coupling, is modeled as the relaxation oscillator

$$
\begin{aligned}
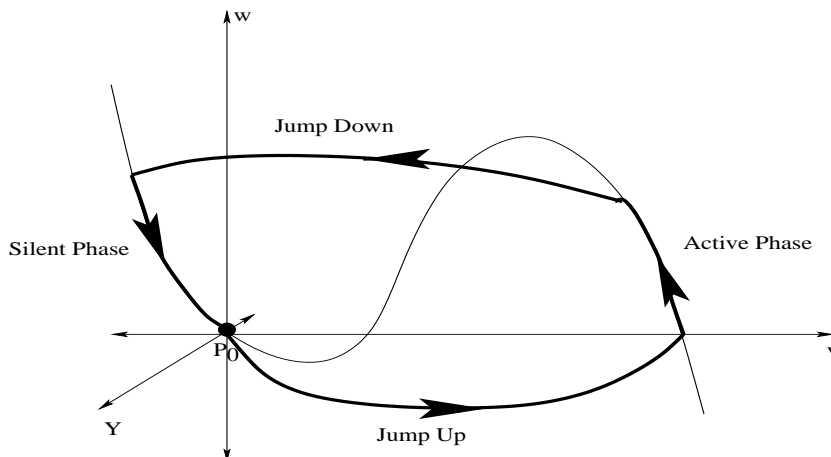v' &= f(v, w) \\
w' &= \epsilon g(v, w)
\end{aligned}
\tag{29}
$$

Figure 13: The singular homoclinic orbit corresponding to a traveling wave solution.

Here ϵ is assumed to be small; that is, w represents a slowly evolving quantity. As in Section 3, we assume that the v-nullcline, $f(v, w) = 0$, defines a cubic-shaped curve and the w-nullcline, $g = 0$, is a monotone increasing curve which intersects $f = 0$ at a unique point p_0. We also assume that $f > 0$ ($f < 0$) below (above) the v-nullcline and $g > 0$ (< 0) below (above) the w-nullcline.

System (29) can be viewed as a simple model for a bursting neuron in which the active phase corresponds to the envelope of a burst's rapid spikes. Of course, a two-dimensional model for a single cell cannot exhibit the more exotic dynamics described in the previous section for a bursting cell. However, by considering a simple relaxation-type oscillator for each cell, we will be able to discuss how network properties contribute to the emergent behavior of a population of cells. It is, of course, a very interesting issue to understand how this population behavior changes when one considers more detailed models for each cell. Some results for more detailed models are given in [30].

In the next section, we describe how we model the two mutually coupled cells. The form of coupling used is referred to as *synaptic coupling* and is meant to correspond to a simple model for chemical synapses. There are many different forms of synaptic coupling. For example, it may be excitatory or inhibitory and it may exhibit either fast or slow dynamics. We are particularly interested in how the nature of the synaptic coupling affects the

34

emergent population rhythm. A natural question is whether excitatory or inhibitory coupling leads to either synchronous or desynchronous rhythms. There are four possible combinations and all four may, in fact, be stably realized, depending on the details of the intrinsic and synaptic properties of the cells. Here we discuss conditions for when excitatory coupling leads to synchronous rhythms and inhibitory coupling leads to antiphase behavior.

5.2 Synaptic Coupling

We model a pair of mutually coupled neurons by the following system of differential equations

$$
\begin{aligned}
v_1' &= f(v_1, w_1) - s_2 g_{syn}(v_1 - v_{syn}) \\
w_1' &= \epsilon g(v_1, w_1) \\
v_2' &= f(v_2, w_2) - s_1 g_{syn}(v_2 - v_{syn}) \\
w_2' &= \epsilon g(v_2, w_2)
\end{aligned}
\tag{30}
$$

Here (v_1, w_1) and (v_2, w_2) correspond to the two cells. The coupling term $s_j g_{syn}(v_i - v_{syn})$ can be viewed as an additional current which may change a cell's membrane potential v_i. The parameter g_{syn} corresponds to the maximal conductance of the synapse and is positive, while the reversal potential v_{syn} determines whether the synapse is excitatory or inhibitory. If $v < v_{syn}$ along each bounded singular solution, then the synapse is excitatory, while if $v > v_{syn}$ along each bounded singular solution, then the synapse is inhibitory.

The terms s_i, $i = 1, 2$, in (30) encode how the postsynaptic conductance depends on the presynaptic potentials v_i. There are several possible choices for the s_i. The simplest choice is to assume that $s_i = H(v_i - \theta_{syn})$, where H is the Heaviside step function and θ_{syn} is a threshold above which one cell can influence the other. Note, for example, that if $v_1 < \theta_{syn}$, then $s_1 = H(v_1 - \theta_{syn}) = 0$, so cell 1 has no influence on cell 2. If, on the other hand, $v_1 > \theta_{syn}$, then $s_1 = 1$ and cell 2 is affected by cell 1.

Another choice for the s_i is to assume that they satisfy a first order equation of the form

$$
s_i' = \alpha(1 - s_i)H(v_i - \theta_{syn}) - \beta s_i
\tag{31}
$$

where α and β are positive constants and H and θ_{syn} are as before. Note that α and β are related to the rates at which the synapses turn on or turn

off. For *fast synapses*, we assume that both of these constants are $O(1)$ with respect to ϵ. For a *slow synapse*, we assume that $\alpha = O(1)$ and $\beta = O(\epsilon)$; hence, a slow synapse activates on the fast time scale but turns off on the slow time scale.

5.3   Geometric Approach

All of the networks in this paper are analyzed by treating ϵ as a small, singular perturbation parameter. As in the previous section, the first step in the analysis is to identify the fast and slow variables. We then dissect the full system of equations into fast and slow subsystems. The fast subsystem is obtained by simply setting $\epsilon = 0$ in the original equations. This leads to a reduced set of equations for the fast variables with each of the slow variables held constant. The slow subsystems are obtained by first introducing the slow time scale $\tau = \epsilon t$ and then setting $\epsilon = 0$ in the resulting equations. This leads to a reduced system of equations for just the slow variables, after solving for each fast variable in terms of the slow ones. The slow subsystems determine the evolution of the slow variables while the cells are in either the active or the silent phase. During this time, each cell lies on either the left or the right branch of some "cubic" nullcline determined by the total synaptic input which the cell receives. This continues until one of the cells reaches the left or right "knee" of its corresponding cubic. Upon reaching a knee, the cell may either jump up from the silent to the active phase or jump down from the active to the silent phase. The jumping up or down process is governed by the fast equations.

For a concrete example, consider two mutually coupled cells with fast synapses. The dependent variables (v_i, w_i, s_i), $i = 1, 2$, then satisfy (30) and (31). The slow equations are

$$
\begin{aligned}
0 &= f(v_i, w_i) - s_j g_{syn}(v_i - v_{syn}) \\
\dot{w}_i &= g(v_i, w_i) \\
0 &= \alpha(1 - s_i)H(v_i - \theta_{syn}) - \beta s_i
\end{aligned}
\tag{32}
$$

where differentiation is with respect to τ and $i \neq j$. The first equation in (32) states that (v_i, w_i) lies on a curve determined by s_j. The third equation states that if cell i is silent $(v_i < \theta_{syn})$, then $s_i = 0$, while if cell i is active, then $s_i = \frac{\alpha}{\alpha + \beta} \equiv s_A$. We demonstrate that it is possible to reduce (32) to a single equation for each of the slow variables w_i. Before doing this, it will be convenient to introduce some notation.

Let $\Phi(v, w, s) \equiv f(v, w) - g_{syn}s(v - v_{syn})$. If g_{syn} is not too large, then each $C_s \equiv \{\Phi(v, w, s) = 0\}$ defines a cubic-shaped curve. We express the left and right branches of C_s by $\{v = \Phi_L(w, s)\}$ and $\{v = \Phi_R(w, s)\}$, respectively. Finally, let

$$G_L(w, s) = g(\Phi_L(w, s), w) \quad \text{and} \quad G_R(w, s) = g(\Phi_R(w, s), w)$$

Now the first equation in (32) can be written as $0 = \Phi(v_i, w_i, s_j)$ with s_j fixed. Hence, $v_i = \Phi_\alpha(w_i, s_j)$ where $\alpha = L$ if cell i is silent and $\alpha = R$ if cell i is active. It then follows that each slow variable w_i satisfies the single equation

$$\dot{w}_i = G_\alpha(w_i, s_j) \tag{33}$$

By dissecting the full system into fast and slow subsystems, we are able to construct singular solutions of (30),(31). In particular, this leads to sufficient conditions for when there exists a singular synchronous solution and when this solution is (formally) asymptotically stable. The second step in the analysis is to rigorously prove that the formal analysis, in which $\epsilon = 0$, is justified for small $\epsilon > 0$. This raises some very subtle issues in the geometric theory of singular perturbations, some of which have not been completely addressed in the literature. For most of the results presented here, we only consider singular solutions.

We note that the geometric approach used here is somewhat different from that used in many dynamical systems studies (see, for example, [28]). All of the networks considered here consist of many differential equations, especially for larger networks. Traditionally, one would interpret the solution of this system as a single trajectory evolving in a very large dimensional phase space. We consider several trajectories, one corresponding to a single cell, moving around in a much lower dimensional phase space (see also [43], [41], [34], [40], [30]). After reducing the full system to a system for just the slow variables, the dimension of the lower dimensional phase space equals the number of slow intrinsic variables and slow synaptic variables corresponding to each cell. In the worst case considered here, there is only one slow intrinsic variable for each cell and one slow synaptic variable; hence, we never have to consider phase spaces with dimension more than two. Of course, the particular phase space we need to consider may change, depending on whether the cells are active or silent and also depending on the synaptic input that a cell receives.

5.4 Synchrony With Excitatory Synapses

Consider two mutually coupled cells with excitatory synapses. Our goal here is to give sufficient conditions for the existence of a synchronous solution and its stability. Note that if the synapses are excitatory, then the curve $C_A \equiv C_{s_A}$ lies 'above' $C_0 \equiv \{f = 0\}$ as shown in Fig. 14. This is because for an excitatory synapse, $v < v_{syn}$ along the synchronous solution. Hence, on C_A, $f(v,w) = g_{syn}s_A(v - v_{syn}) < 0$, and we are assuming that $f < 0$ above C_0. If g_{syn} is not too large, then both C_0 and C_A will be cubic shaped. We assume that the threshold θ_{syn} lies between the two knees of C_0. In the statement of the following result, we denote the left knee of C_0 by (v_{LK}, w_{LK}).

Theorem: Assume that each cell, without any coupling, is oscillatory. Moreover, assume the synapses are fast and excitatory. Then there exists a synchronous periodic solution of (30), (31). This solution is asymptotically stable if one of the following two conditions is satisfied.

(H1) $\frac{\partial f}{\partial w} < 0$, $\frac{\partial g}{\partial v} > 0$, and $\frac{\partial g}{\partial w} < 0$ near the singular synchronous solution.

(H2) $|g(v_{LK}, w_{LK})|$ is sufficiently small.

Remark 5.1 We note that the synchronous solution cannot exist if the cells are excitable and the other hypotheses, concerning the synapses, are satisfied. This is because along a synchronous solution, each (v_i, w_i) lies on the left branch of C_0 during the silent phase. If the cells are excitable, then each (v_i, w_i) will approach the point where the w-nullcline $\{g = 0\}$ intersects the left branch of C_0. The cells, therefore, will not be able to jump up to the active phase.

Remark 5.2 The assumptions concerning the partial derivatives of f and g in (H1) are not very restrictive since we are already assuming that $f > 0$ (< 0) below (above) the v-nullcline and $g > 0$ (< 0) below (above) the w-nullcline.

Remark 5.3 A useful way to interpret (H2) is that the silent phases of the cells are much longer than their active phases. This is because $g(v_{LK}, w_{LK})$ gives the rate at which the slow variables w_i evolve near the end of the silent phase. Note that $g(v_{LK}, w_{LK})$ will be small if the left knee of C_0 is very close to the w-nullcline.

Proof: We first consider the existence of the synchronous solution. This is straightforward because along a synchronous solution $(v_1, w_1, s_1) = (v_2, w_2, s_2) \equiv (v, w, s)$ satisfy the reduced system

$$
\begin{aligned}
v' &= f(v, w) - sg_{syn}(v - v_{syn}) \\
w' &= \epsilon g(v, w) \\
s' &= \alpha(1 - s)H(v - \theta_{syn}) - \beta s
\end{aligned}
$$

The singular solution consists of four pieces. During the silent phase, $s = 0$ and (v, w) lies on the left branch of C_0. During the active phase $s = s_A$ and (v, w) lies on the right branch of C_A. The jumps between these two phases occur at the left and right knees of the corresponding cubics.

We next consider the stability of the synchronous solution to small perturbations. We begin with both cells close to each other in the silent phase on the left branch of C_0, with cell 1 at the left knee ready to jump up. We follow the cells around in phase space by constructing the singular solution until one of the cells returns to the left knee of C_0. As before, the singular solution consists of four pieces. We need to show that the cells are closer to each other after this complete cycle than they were initially.

The first piece of the singular solution begins when cell 1 jumps up. When $v_1(t)$ crosses θ_{syn}, $s_1(t) \to s_A$. This raises the cubic corresponding to cell 2 from C_0 to C_A. If $|w_1(0) - w_2(0)|$ is sufficiently small, corresponding to a sufficiently small perturbation, then cell 2 lies below the left knee of C_A. The fast equations then force cell 2 to also jump up to the active phase, as shown in Fig. 14. Note that this piece takes place on the fast time scale. Hence, on the slow time scale, both cells jump up at precisely the same time.

During the second piece of the singular solution, both oscillators lie in the active phase on the right branch of C_A. Note that the ordering in which the oscillators track along the left and right branches has been reversed. While in the silent phase, cell 1 was ahead of cell 2. In the active phase, cell 2 leads the way. The oscillators remain on the right branch of C_A until cell 2 reaches the right knee.

The oscillators then jump down to the silent phase. Cell 2 is the first to jump down. When $v_2(t)$ crosses θ_{syn}, s_2 switches from s_A to 0 on the fast time scale. This lowers the cubic corresponding to cell 1 from C_A to C_0. If, at this time, cell 1 lies above the right knee of C_A, then cell 1 must jump down to the silent phase. This will certainly be the case if the cells are initially close enough to each other.

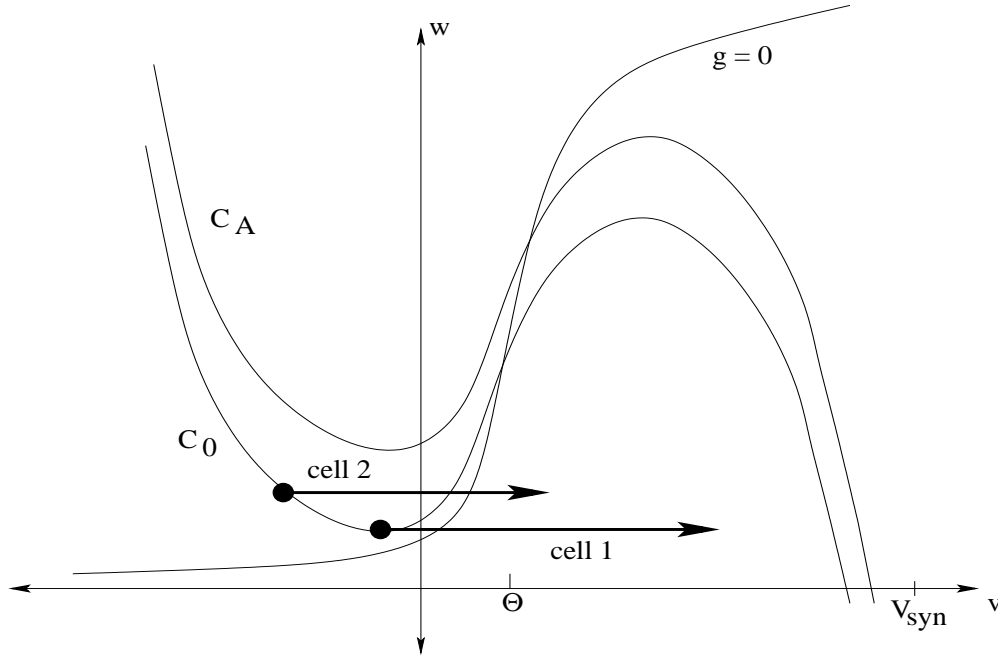During the final piece of the singular solution, both oscillators move

Figure 14: Nullclines for an oscillatory relaxation oscillator with (C_A) and without (C_0) excitatory coupling. Note that cell 2 responds to cell 1 through Fast Threshold Modulation.

down the left branch of C_0 until cell 1 reaches the left knee. This completes one full cycle.

To prove that the synchronous solution is stable, we must show that the cells are closer to each other after this cycle; that is, there is compression in the distance between the cells. There are actually several ways to demonstrate this compression; these correspond to two different ways to define what is meant by the 'distance' between the cells. Here we consider a Euclidean metric, which is defined as follows: Suppose that both cells lie on the same branch of the same cubic and the coordinates of cell i are (v_i, w_i). Then the distance between the cells is defined as simply $|w_1 - w_2|$. Note that during the jump up and the jump down, this metric remains invariant. This is because the jumps are horizontal so the values of w_i do not change. If there is compression, therefore, it must take place as the cells evolve in the silent and active phases. We now show that this is indeed the case if (H1) is satisfied.

40

Suppose that when $\tau = 0$, both cells lie in the silent phase on C_0. We assume, for convenience, that $w_2(0) > w_1(0)$. We need to prove that $w_2(\tau) - w_1(\tau)$ decreases as long as the cells remain in the silent phase. Now each w_i satisfies (33) with $\alpha = L$ and $s_j = 0$. Hence,

$$w_i(\tau) \;=\; w_i(0) \;+\; \int_0^\tau G_L(w_i(\xi), 0) d\xi$$

and, using the Mean Value Theorem,

$$
\begin{aligned}
w_2(\tau) - w_1(\tau) &= w_2(0) - w_1(0) \\
&\quad + \int_0^\tau G_L(w_2(\xi), 0) - G_L(w_1(\xi), 0) \; d\xi \\
&= w_2(0) - w_1(0) \\
&\quad + \int_0^\tau \frac{\partial G_L}{\partial w}(w^*, 0)(w_2(\xi) - w_1(\xi)) d\xi
\end{aligned}
\tag{34}
$$

for some w^*. Now $G_L(w, s) = g(\Phi_L(w), w)$. Hence, $\frac{\partial G_L}{\partial w} = g_v \Phi_L'(w) + g_w$. We assume in (H1) that $g_v > 0$ and $g_w < 0$ near the synchronous solution. Moreover, $\Phi_L'(w) < 0$ because $v = \Phi_L(w)$ defines the left branch of the cubic C_0 which has negative slope. It follows that $\frac{\partial G_L}{\partial w} < 0$, and therefore, from (34), $w_2(\tau) - w_1(\tau) < w_2(0) - w_1(0)$. This gives the desired compression; a similar computation applies in the active phase. We note that if there exists $\gamma > 0$ such that $\frac{\partial G_L}{\partial w} < -\gamma$ along the left branch, then Gronwall's inequality shows that $w_2(\tau) - w_1(\tau)$ decreases at an exponential rate.

We next consider (H2) and demonstrate why this leads to compression of trajectories. Suppose, for the moment, that $g(v_{LK}, w_{LK}) = 0$; that is, the left knee of C_0 touches the w-nullcline at some fixed point. Then both cells will approach this fixed point as they evolve along the left branch of C_0 in the silent phase. There will then be an infinite amount of compression, since both cells approach the same fixed point. It follows that we can assume that the compression is as large as we please by making $g(v_{LK}, w_{LK})$ sufficiently small. If the compression is sufficiently large, then it will easily dominate any possible expansion over the remainder of the cells' trajectories. This will, in turn, lead to stability of the synchronous solution.

Remark 5.4 The mechanism by which one cell fires, and thereby raises the cubic of the other cell such that it also fires, was referred to as *Fast Threshold Modulation (FTM)* in [34]. There, a time metric was introduced to establish the compression of trajectories of excitatorily coupled cells, which implies

the stability of the synchronous solution. A detailed discussion of the time metric can be found in [20]; see also [23].

Remark 5.5 While the synchronous solution has been shown to be stable, it need not be globally stable. In [21], it is shown that this network may exhibit stable antiphase solutions if certain assumptions on the parameters and nonlinear functions are satisfied.

We have so far considered a completely homogeneous network with just two cells. The analysis generalizes to larger inhomogeneous networks in a straightforward manner, if the degree of heterogeneity between the cells is not too large. The major difference in the analysis is that, with heterogeneity, the cells may lie on different branches of different cubics during the silent and active phases. The resulting solution cannot be perfectly synchronous; however, as demonstrated in [43], one can often expect synchrony in the jump-up, but not in the jump-down. Related work on heterogeneous networks include [35], [26], [4].

One may also consider, for example, an arbitrarily large network of identical oscillators with nearest neighbor coupling. We do not assume that the strength of coupling is homogeneous. Suppose that we begin the network with each cell in the silent phase. If the cells are identical, then they must all lie on the left branch of C_0. Now if one cell jumps up it will excite its neighbors and raise their corresponding cubics. If the cells begin sufficiently close to each other, then these neighbors will jump up due to FTM. In a similar manner, the neighbor's neighbors will also jump due to FTM and so on until every cell jumps up. In this way, every cell jumps up at the same (slow) time. While in the active phase, the cells may receive different input and, therefore, lie on the right branches of different cubics. Once one of the cells jumps down, there is no guarantee that other cells will also jump down at this (slow) time, because the cells to which it is coupled may still receive input from other active cells. Hence, one cannot expect synchrony in the jumping down process. Eventually every cell must jump down. Note that there may be considerable expansion in the distance between the cells in the jumping down process. If $|g(v_{LK}, w_{LK})|$ is sufficiently small, however, as in the previous result, then there will be enough compression in the silent phase so that the cells will still jump up together. Here we assumed that the cells are identical; however, the analysis easily follows if the heterogeneities among the cells are not too large. A detailed analysis of this network is given in [43].

5.5 Desynchrony With Inhibitory Synapses

We now consider two mutually coupled cells with inhibitory synapses. Under this coupling, the curve C_A now lies below C_0. As before, we assume that g_{syn} is not too large, such that both C_0 and C_A are cubic shaped. We also assume that the right knee of C_A lies above the left knee of C_0 as shown in Fig. 15. Some assumptions on the threshold θ_{syn} are also required. For now, we assume that θ_{syn} lies between the left knee of C_0 and right knee of C_A.

We will assume throughout this section that the synapses are fast and inhibitory. The main results state that if a synchronous solution exists then it must be unstable. The network will typically exhibit either out-of-phase oscillations or a completely quiescent state and we give sufficient conditions for when either of these arises. We note that the network may exhibit bistability; both the out-of-phase and completely quiescent solutions may exist and be stable for the same parameter values. These results are all for singular solutions. Some rigorous results for $\epsilon > 0$ are given in [41].

The first result concerns the existence and stability of the synchronous solution.

Theorem: Assume that the synapses are fast and inhibitory. If each cell, without any coupling, is oscillatory and θ_{syn} is sufficiently large, then there exists a singular synchronous solution. This solution is unstable. If each cell, without any coupling, is excitable, then there does not exist a singular synchronous solution.

Proof: The existence of a singular synchronous solution for oscillatory cells follows precisely as in the previous section. During the silent phase, the trajectory lies on the left branch of C_0, while in the active phase it lies on the right branch of C_A. Note that we require that the right knee of C_A lies above the left knee of C_0. Moreover, when the synchronous solution jumps up and crosses the threshold $v = \theta_{syn}$, it should lie to the right of the middle branch of C_A; otherwise, it would fall down to the silent phase. This is why we assume that θ_{syn} is sufficiently large.

This solution is unstable for the following reason. Suppose both cells are initially very close to each other on C_0. The cells then evolve on C_0 until one of the cells, say cell 1, reaches the left knee of C_0. Cell 1 then jumps up to the active phase. When v_1 crosses the threshold θ_{syn}, s_1 switches from 0 to s_A and cell 2 jumps from C_0 to C_A, as shown in Fig. 15. This demonstrates that the cells are uniformly separated for arbitrarily close initial data. The synchronous solution must, therefore, be unstable.

The synchronous solution cannot exist if the cells are excitable for precisely the same reason discussed in the previous section. If such a solution did exist then each cell would lie on C_0 during its silent phase. Each cell would then approach the stable fixed point on this branch and would never be able to jump up to the active phase.

We next consider out-of-phase oscillatory behavior. One interesting feature of mutually coupled networks is that such oscillations can arise even if each cell is excitable for fixed levels of synaptic input. The following theorem gives sufficient conditions for when this occurs. We will require that the active phase of the oscillation is sufficiently long. To give precise conditions, we introduce the following notation.

Assume that the left and right knees of C_0 are at (v_{LK}, w_{LK}) and (v_{RK}, w_{RK}), respectively. If the w-nullcline intersects the left branch of C_A, then we denote this point by $(v_A, w_A) = p_A$. We assume that $w_A < w_{LK}$. Let τ_L be the (slow) time it takes for the solution of (33) with $\alpha = L$ and $s = s_A$ to go from $w = w_{RK}$ to $w = w_{LK}$, and let τ_R be the time it takes for the solution of (33) with $\alpha = R$ and $s = 0$ to go from $w = w_{LK}$ to $w = w_{RK}$. Note that τ_L is related to the time a solution spends in the silent phase, while τ_R is related to the time a solution spends in the active phase.

Theorem: Assume that the cells are excitable for each fixed level of synaptic input and the synapses are fast, direct, and inhibitory. Moreover, assume that $w_A < w_{LK}$ and $\tau_L < \tau_R$. Then the network exhibits stable out-of-phase oscillatory behavior.

Remark 5.6 We do not claim that the out-of-phase solution is uniquely determined or that it corresponds to antiphase behavior. These results may hold; however, their proofs require more analysis than that given here.

Remark 5.7 The rest state with each cell at the fixed point on C_0 also exists and is stable. Hence, if the hypotheses of Theorem are satisfied, then the network exhibits bistability.

Proof: Suppose that we begin with cell 1 at the right knee of C_0 and cell 2 on the left branch of C_A with $w_A < w_2(0) < w_{LK}$. Then cell 1 jumps down and, when v_1 crosses the threshold θ_{syn}, cell 2's cubic switches from C_A to C_0. Since $w_2(0) < w_{LK}$, cell 2 lies below the left knee of C_0, so it must jump up to the active phase. After these jumps, cell 1 lies on the left branch of C_A, while cell 2 lies on the right branch of C_0.
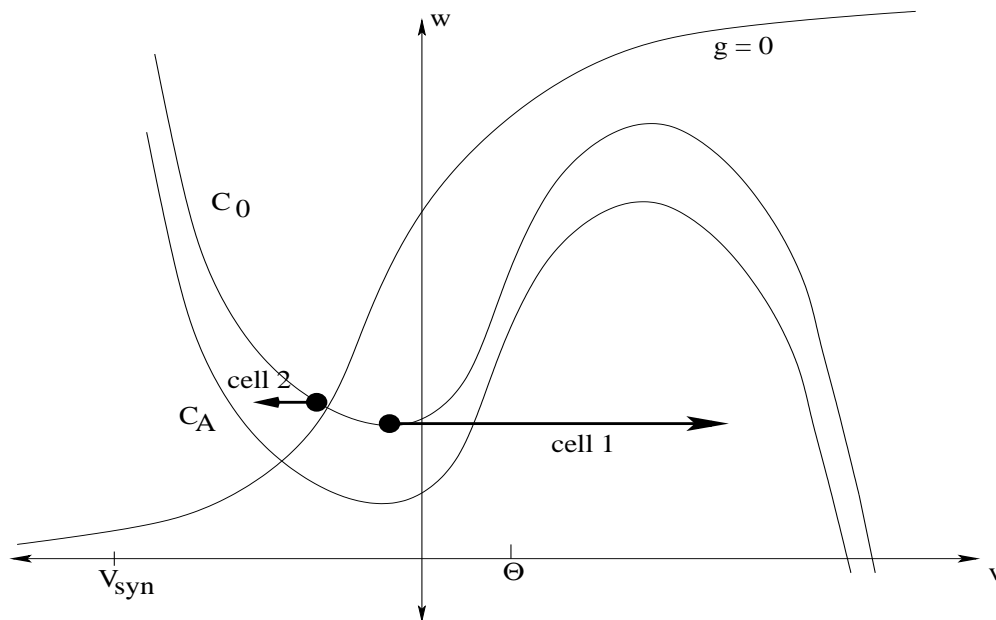
Figure 15: Instability induced by mutual inhibition. Cell 2 jumps to C_A when cell 1 fires.

Cell 2 then moves up the right branch of C_0 while cell 1 moves down the left branch of C_A, approaching p_A. This continues until cell 2 reaches the right knee of C_0 and jumps down. We claim that at this time, cell 1 lies below the left knee of C_0, so it must jump up. We can then keep repeating this argument to obtain the sustained out-of-phase oscillations. The reason why cell 1 lies below the left knee of C_0 when cell 2 jumps down is because it spends a sufficiently long amount of time in the silent phase. To estimate this time, note that because cell 2 was initially below the left knee of C_0, the time it spends in the active phase before jumping down is greater than τ_R. Hence, the time cell 1 spends in the silent phase from the time it jumps down is greater than $\tau_R > \tau_L$. From the definitions, since cell 1 was initially at the right knee of C_0, it follows that cell 1 must be below the left knee of C_0 when cell 2 jumps down, which is what we wished to show.

Remark 5.8 Wang and Rinzel [45] distinguish between "escape" and "release" in producing out-of-phase oscillations. In the proof of the preceding theorem, the silent cell can only jump up to the active phase once the active cell jumps down and releases the silent cell from inhibition. This is referred

to as the release mechanism and is often referred to as *post inhibitory rebound* [9]. To describe the escape mechanism, suppose that each cell is oscillatory for fixed levels of synaptic input. Moreover, one cell is active and the other is inactive. The inactive cell will then be able to escape the silent phase from the left knee of its cubic, despite the inhibition it receives from the active cell. Note that when the silent cell jumps up, it inhibits the active cell. This lowers the cubic of the active cell, so it may be forced to jump down before reaching a right knee.

Remark 5.9 We have presented rigorous results that demonstrate that excitation can lead to synchrony and inhibition can lead to desynchrony. These results depended on certain assumptions, however. We assumed, for example, that the synapses turned on and off on a fast time scale; moreover, the results hold in some singular limit. In is, in fact, possible for excitatory synapses to generate stable desynchronous oscillations and for inhibitory synapses to generate stable synchronous oscillations. Conditions for when these are possible has been the subject of numerous research articles. References may be found in [40].

Remark 5.10 The two cell model (30) can generate other rhythms besides those discussed so far. For example, it is possible that one cell periodically fires action potentials, while the other cell is always silent. This is sometimes refereed to as a *suppressed solution.* It arises if the rate at which inhibition turns off is slower than the rate at which a cell recovers in the silent phase. That is, suppose cell 1 fires. This sends inhibition to cell 2, preventing it from firing. Now if cell 1 is able to recover from its silent phase before the inhibition to cell 2 wears off, then cell 1 will fire before cell 2 is able to. This will complete one cycle and cell 2 will continue to be suppressed. If the time for cells to recover in the silent phase is comparable to the time for inhibition to decay, then more exotic solutions are possible (see [40]).

6   Activity Patterns in the Basal Ganglia

6.1   Introduction

In this final chapter, we discuss a recent model for neuronal activity patterns in the basal ganglia [42]. This is a part of the brain believed to be involved in the control of movement. Dysfunction of the basal ganglia is associated with movement disorders such as Parkinson's disease and Huntington's disease. Neurons within the basal ganglia are also the target of recent surgical

procedures, including deep brain stimulation. An introduction to the basal ganglia can be found in [18].

The issues discussed arise in numerous other neuronal systems. We shall describe how these large neuronal networks are modeled, what population rhythms may arise in these networks and the possible roles of these activity patterns.

6.2   The Basal Ganglia

The basal ganglia consist of several nuclei; these are illustrated in Fig. 16. The primary input nucleus is the striatum; it receives motor information from the cortex. The primary output nuclei are the internal segment of the globus pallidus (GPi) and the substantia nigra par retularis (SNr). Neuronal information passes through the basal ganglia through two routes. The direct pathway passes directly from the striatum to the output nuclei. In the indirect pathway, the information passes from the striatum to the external segment of the globus pallidus (GPe) onto the subthalamic nuclues (STN) and then onto the output nuclei. The final nucleus is the substantia nigra par compacta (SNc). This is the primary source of dopamine.

Fig. 16 illustrates that some of the pathways within the basal ganglia are excitatory and some are inhibitory. Most of the pathways are inhibitory except for those that originate in the STN. Note that the pathways arising from SNc are labeled both inhibitory and excitatory. This is because there are different classes of dopamine receptors within the striatum. We also note that Fig. 16 illustrates only some of the pathways reported in the literature.
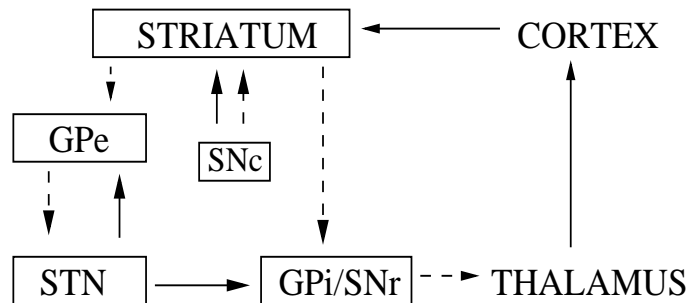

Figure 16: Nuclei within the basal ganglia. Solid arrows indicate excitatory connections and dashed arrows indicate inhibitory connections

Parkinson's disease is associated with a severe reduction of dopamine.

Experiments have also demonstrated that during Parkinson's disease, there is a change in the neuronal activity of the output nucleus GPi. Previous explanations for how a loss of dopamine leads to altered neuronal activity in GPi have been in terms of an average firing rate of neurons; that is, the average number of action potentials in some fixed interval of time. A detailed description of this explanation can be found in [1, 8, 42]. It has been successful in accounting for some features of PD; however, it cannot account for others. For example, it is not at all clear how one can explain tremor. It also cannot account for recent experiments that demonstrate that there is an increased level synchronization among neurons in the STN and GPi during a parkinsonian state [14]. Several authors have suggested that the pattern of neuronal activity, not just the firing rate, is crucially important.

The goal of the modeling study in [42] is to test hypotheses on how the loss of dopamine may lead to tremor-like oscillations and changes in firing patterns. We construct a model for neurons within GPe and STN based on recent experiments [2]. We use computational methods to study the types of activity patterns that arise in this model. In particular, we demonstrate that the model can exhibit irregular uncorrelated patterns, synchronous tremor-like rhythms, and propagating wave-like activity. In the next subsection, we describe the computational model. We then describe the types of activity patterns that arise in the model.

6.3   The Model

Here we describe the model for the STN and GPe network. The detailed equations are given in [42]. These equations are derived using the Hodgkin-Huxley formalism discussed earlier. The precise equations are different from the Hodgkin-Huxley equations, however. This is because the STN and GPe neurons contain channels different from those in the squid's giant axon. In particular, calcium plays a very important role in generating the action potential of STN and GPe neurons. There are two types of potassium channels, one of which depends on the concentration of intracellular calcium (along with membrane potential). There are also two types of calcium channels in STN neurons.

The membrane potential of each STN neuron obeys the current balance equation:

$$C_m \frac{dV}{dt} \;=\; -I_L - I_K - I_{Na} - I_T - I_{Ca} - I_{AHP} - I_{G \to S} \,.$$

The leak current is given by $I_L = g_L(v - v_L)$, and the other voltage-dependent currents are described by the Hodgkin-Huxley formalism as fol-

lows: $I_K = g_K n^4 (v - v_K)$, $I_{Na} = g_{Na} m_\infty^3(v) h(v - v_{Na})$, $I_T = g_T a_\infty^3(v) b_\infty^2(r)(v - v_{Ca})$, and $I_{Ca} = g_{Ca} s_\infty^2(v)(v - v_{Ca})$. The slowly-operating gating variables n, h, and r are treated as functions of both time and voltage, and have first order kinetics governed by differential equations of the form $\frac{dX}{dt} = \phi_X \frac{(X_\infty(v) - X)}{\tau_X(v)}$ (where X can be n, h, or r), with $\tau_X(v) = \tau_X^0 + \frac{\tau_X^1}{1 + \exp[-(v - \theta_X^\tau)/\sigma_X^\tau]}$. Activation gating for the rapidly activating channels (m, a, and s) was treated as instantaneous. For all gating variables $X = n, m, h, a, r$, or s, the steady state voltage dependence was determined using $X_\infty(v) = \frac{1}{1 + \exp[-(v - \theta_X)/\sigma_X]}$. The gating variable b was modeled in a similar, but somewhat different, manner; we do not describe this here. As the final intrinsic current, we take $I_{AHP} = g_{AHP}(v - v_K) \frac{[Ca]}{([Ca] + k_1)}$ where $[Ca]$, the intracellular concentration of Ca^{2+} ions, is governed by $[Ca]' = \epsilon (-I_{Ca} - I_T - k_{Ca}[Ca])$.

The current $I_{G \to S}$ that represents synaptic input from the GPe to STN is modeled as $I_{G \to S} = g_{G \to S}(v - v_{G \to S}) \sum s_j$. The summation is taken over the presynaptic GPe neurons, and each synaptic variable s_j solves a first order differential equation $s_j' = \alpha H_\infty(vg_j - \theta_g)(1 - s_j) - \beta s_j$. Here vg_j is the membrane potential of the GPe neuron j, and $H_\infty(v) = 1/\left(1 + \exp\left[-(v - \theta_g^H)/\sigma_g^H\right]\right)$.

The precise forms of the nonlinear functions in this model, along with parameter values, are given in [42]. The GPe neurons are modeled in a similar way. We do not describe these equations here.

The model STN neurons were adjusted to exhibit properties that are characteristic of the firing of STN neurons in experiments [2]. Fig. 17, left column, shows the firing properties of the model STN neurons. These cells fire intrinsically at approximately 3 Hz and exhibit high frequency sustained firing and strong rebound bursts after release from hyperpolarizing current. Fig. 17, right column, illustrates the firing properties of single GPe neurons. These cells can fire rapid periodic spikes with sufficient applied current. They also display bursts of activity when subjected to a small constant hyperpolarizing current.

Currently the details of connections between STN and GPe cells are poorly understood. It is known that STN neurons provide one of the largest sources of excitatory input to the globus pallidus and that the GPe is a major source of inhibitory afferents to the STN. However, the spatial distribution of axons in each pathway, as well as the number of cells innervated by single neurons in each direction, are not known to the precision required for a computer model. Therefore, in [42] we consider multiple architectures in order to study what types of activity patterns may arise in a particular class of network architecture.. In the model networks, each GPe neuron
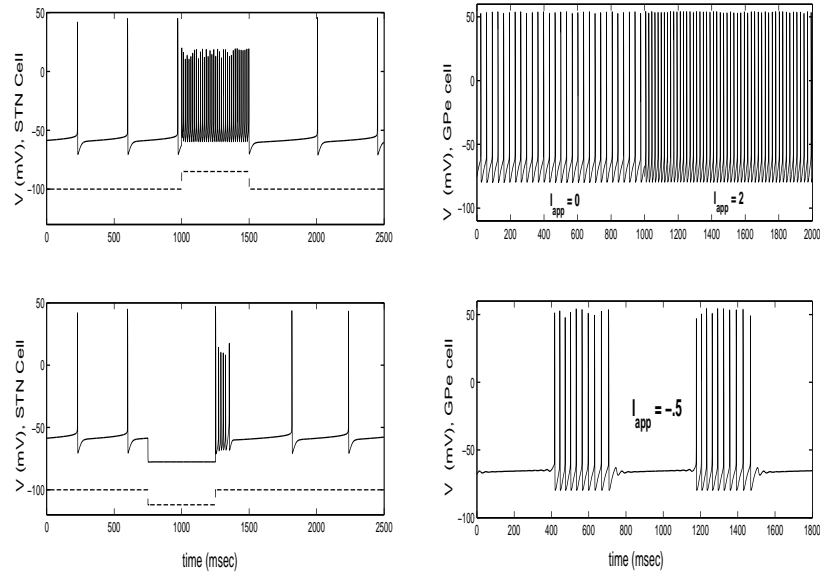
49

Figure 17: Voltage traces for (left) STN and (right) GPe neurons for different levels of applied current. STN cells display high frequency sustained firing with higher input (as shown by the elevated dashed line) and fire rebound bursts after release from hyperpolarizing current. GPe cells fire rapid periodic spikes for positive input and fire bursts of spikes for small negative applied current.

sends inhibition to other GPe neurons as well as to one or more STN neurons. Each STN neuron sends excitation to one or more GPe neurons. A prototype network is illustrated in Figure 18.
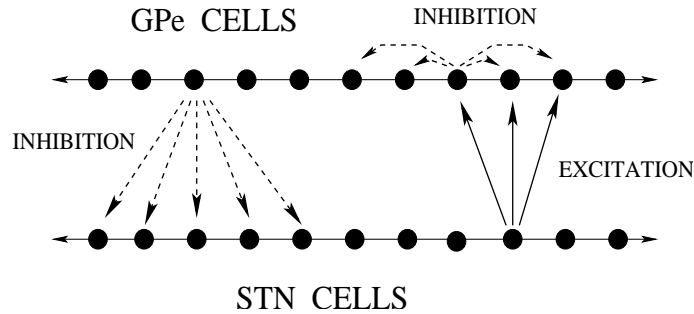

Figure 18: Architecture of the STN/GPe network.

6.4   Activity Patterns

Two activity patterns displayed by the model are shown in Fig. 19. The left column displays irregular and weakly correlated firing of each cell. The voltage traces of two STN neurons are shown. shown. Irregular activity arises in sparsely connected, unstructured networks in which each neuron is synaptically connected to only a small number of other neurons chosen at random. It is possible for irregular activity to also arise in structured networks, however.

The right column of Fig. 18 displays clustered activity, in which each structure is divided into subsets of neurons that become highly correlated with each other. The most commonly observed clustered pattern consists of two clusters, with alternating pairs of cells belonging to opposite clusters. Different clusters alternate firing, and in this pattern, cluster membership is persistent over time. Both episodic and continuous clustering are possible. Clustered activity typically arises in networks with a structured, sparsely connected architecture.

A third type of activity pattern is traveling waves (not shown). Propagating wave-like activity can be very robust and exist over a wide range of parameter values. They typically arise in networks with a structured, tightly connected architecture. The speed of the wave depends on both the footprint of network architecture and both intrinsic and synaptic time-scales.

We note that both of the patterns shown in Fig. 19 are generated for a network with exactly the same architecture. In order to switch from the irregular pattern to the synchronous pattern, we increase the applied current to the GPe cells (this corresponds to input from the striatum) and the level of intra-GPe inhibition.

6.5   Concluding Remarks

We have shown that in a biophysical, conductance-based model that the cellular properties of the STN and GPe cells can give rise to a variety of rhythmic or irregular self-sustained firing patterns, depending on both the arrangement of connections among and within the nuclei and the effective strengths of the connections. The dependence on network architecture points out the importance of certain missing pieces of anatomical information. It is important to determine the precision of the spatial organization of connections between the STN and GPe neurons and whether the two nuclei project on each other in a reciprocal or out of register manner.

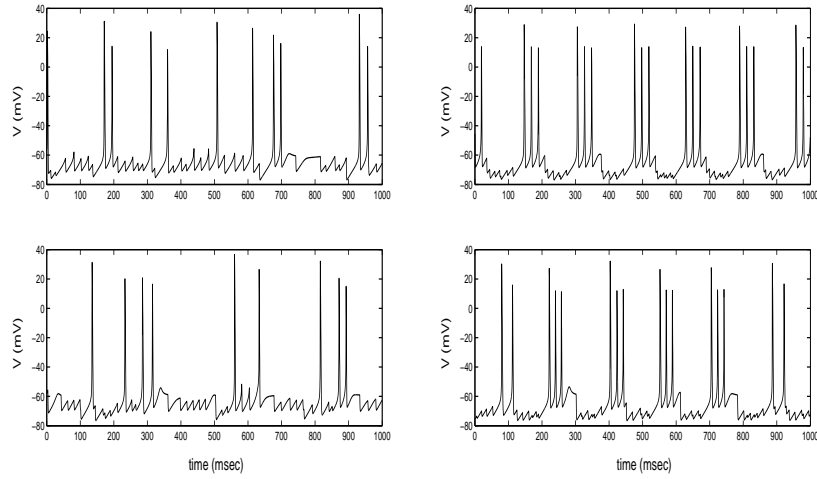According to recent studies, correlated oscillatory activity in the GPe and

Figure 19: Irregular and clustered patterns. Each column shows the voltage traces of two STN neurons.

STN neurons is closely related to the generation of the symptoms of Parkinsonism. Previous firing rate models hold that during Parkinsonian states, an increased level of inhibition from the striatum to GPe causes a decrease in the activity of GPe. This in turn would send less inhibition to STN, thus increasing STN activity and ultimately leading to increased inhibitory output from the basal ganglia to the thalamus. In our model network, a more complex picture emerges, in which the STN and GPe are spontaneously oscillatory and synchronous, whereas intra-GPe inhibition and appropriate level of input from the striatum can act to suppress rhythmic behavior.

The analysis described in earlier chapters is extremely useful in understanding the mechanisms responsible for the generation of the different firing patterns arising in the STN/GPe model. The simple two-cell models considered earlier illustrate, for example, that inhibition may play multiple roles in the generation of activity patterns. In the clustered rhythm, for example, active STN neurons need moderate levels of feedback inhibition from GPe to synchronize among themselves. Silent STN neurons, on the other hand, are prevented from firing because they receive more powerful tonic inhibition. For the generation of propagating waves, intra-GPe inhibition is needed to prevent activity from persisting in the wake of the wave. Hence, this inhibition helps to organize the network into a structured activity pattern. If one increases the intra-GPe inhibition, this can desynchronize the GPe oscillations and irregular firing may result.

The STN/GPe model is an example of an excitatory-inhibitory network. This type of model arises in other neuronal systems. For example, recent models for thalamic sleep rhythms share many of the properties of the STN/GPe model. References to papers on the thalamic sleep rhythms can be found in [31].

References

[1] R.L. Albin, A.B. Young, and J.B. Penney. The functional anatomy of basal ganglia disorders. *Trends in Neurosci.*, **12**:366–375, 1989.

[2] M.D. Bevan and C.J. Wilson. Mechanisms underlying spontaneous oscillation and rhythmic firing in rat subthalamic neurons. *J. Neurosci.*, **19**:7617–7628, 1999.

[3] R.J. Butera, J. Rinzel, and J.C. Smith. Models of respiratory rhythm generation in the pre-Botzinger complex: I. Bursting pacemaker model. *J. Neurophysiology*, **82**:382–397, 1999.

[4] R.J. Butera, J. Rinzel, and J.C. Smith. Models of respiratory rhythm generation in the pre-Botzinger complex: II. Populations of coupled pacemaker neurons. *J. Neurophysiology*, **82**:398–415, 1999.

[5] T.R Chay and J. Keizer. Minimal model for membrane oscillations in the pancreatic β-cell. *Biophys. J.*, **42**:181–190, 1983.

[6] T.R. Chay and J. Rinzel. Bursting, beating, and chaos in an excitable membrane model. *Biophys. J.*, **47**:357–366, 1985.

[7] G. de Vries and R.M. Miura. Analysis of a class of models of bursting electrical activity in pancreatic β-cells. *SIAM J. Appl. Math.*, **58**:607–635, 1998.

[8] M.R. DeLong. Activity of pallidal neurons during movement. *J. Neurophysiol.*, **34**:414–427, 1971.

[9] W. Friesen. Reciprocal inhibition, a mechanism underlying oscillatory animal movements. *Neurosci. Behavior*, **18**:547–553, 1994.

[10] D. Golomb, X.-J. Wang, and J. Rinzel. Synchronization properties of spindle oscillations in a thalamic reticular nucleus model. *J. Neurophysiol.*, **72**:1109–1126, 1994.

[11] J.L Hindmarsh and R.M. Rose. A model of neuronal bursting using three coupled first order differential equations. *Proc. R. Soc. Lond., Ser. B*, **221**:87–102, 1984.

[12] A.L. Hodgkin and A.F. Huxley. A quantitative description of membrane current and its application to conduction and excitation in a nerve. *Journal of Physiology*, **117**:165–181, 1952.

[13] F.C. Hoppensteadt and E.M. Izhikevich. *Weakly Connected Neural Networks*. Springer-Verlag, New York, Berlin, and Heidelberg, 1997.

[14] J.M. Hurtado, C.M. Gray, L.B. Tamas, and K.A. Sigvardt. Dynamics of tremor-related oscillations in the human globus pallidus: A single case study. *Proc. Natl. Acad. Sci. USA*, **96**:1674–1679, 1999.

[15] E.M. Izhikevich. Neural excitability, spiking, and bursting. *International Journal of Bifurcation and Chaos*, **10**, 2000.

[16] D. Johnston and S. M-S. Wu. *Foundations of Cellular Neurophysiology*. MIT Press, Cambridge, Ma. and London, 1997.

[17] C.K.R.T. Jones. Stability of the traveling wave solutions of the fitzhugh-nagumo system. *Trans. Amer. Math. Soc.*, 286:431–469, 1984.

[18] E.R. Kandel, J.H. Schwartz, and T.M. Jessell. *Principles of Neural Science*. Appleton & Lange, Norwalk, Conn., 1991.

[19] J. Keener and J. Sneyd. *Mathematical Physiology*. Springer, New York, Berlin, Heidelberg, 1998.

[20] N. Kopell and B. Ermentrout. Mechanisms of phase-locking and frequency control in pairs of coupled neural oscillators. In B. Fiedler, G. Iooss, and N. Kopell, editors, *Handbook of Dynamical Systems, vol. 3: Towards Applications*. Elsevier, 2003.

[21] N. Kopell and D. Somers. Anti-phase solutions in relaxation oscillators coupled through excitatory synapses. *J. Math. Biol.*, **33**:261–280, 1995.

[22] E. Lee and D. Terman. Uniqueness and stability of periodic bursting solutions. To appear in *Journal of Differential Equations*.

[23] T. LoFaro and N. Kopell. Timing regulation in a network reduced from voltage-gated equations to a one-dimensional map. *J. Math. Biol.* To appear.

[24] C. Morris and H. Lecar. Voltage oscillations in the barnacle giant muscle fiber. *Biophys. J.*, **35**:193–213, 1981.

[25] M. Pernarowski. Fast subsystem bifurcations in a slowly varying Lienard system exhibiting bursting. *SIAM J. Appl. Math.*, **54**:814–832, 1994.

[26] P. Pinsky and J. Rinzel. Intrinsic and network rhythmogenesis in a reduced Traub model for CA3 neurons. *J. Comput. Neurosci.*, **1**:39–60, 1994.

[27] J. Rinzel. A formal classification of bursting mechanisms in excitable systems. In A.M. Gleason, editor, *Proceedings of the International Congress of Mathematicians*, pages 1578–1594. American Mathematical Society, Providence, RI, 1987.

[28] J. Rinzel and G.B. Ermentrout. Analysis of neural excitability and oscillations. In C.Koch and I. Segev, editors, *Methods in Neuronal Modeling: From Ions to Networks*, pages 251–291. The MIT Press, Cambridge, MA, second edition, 1998.

[29] J. Rinzel, D. Terman, X.-J. Wang, and B. Ermentrout. Propagating activity patterns in large-scale inhibitory neuronal networks. *Science*, **279**:1351–1355, 1998.

[30] J. Rubin and D. Terman. Geometric analysis of population rhythms in synaptically coupled neuronal networks. *Neural Comput.*, **12**:597–645, 2000.

[31] J. Rubin and D. Terman. Geometric singular perturbation analysis of neuronal dynamics. In B. Fiedler, G. Iooss, and N. Kopell, editors, *Handbook of Dynamical Systems, vol. 3: Towards Applications*. Elsevier, 2003.

[32] A. Sherman. Contributions of modeling to understanding stimulus-secretion coupling in pancreatic β-cells. *American. J. Phyciology*, **271**:547–559, 1996.

[33] P. Smolen, D. Terman, and J. Rinzel. Properties of a bursting model with two slow inhibitory variables. *SIAM J. Appl. Math.*, **53**:861–892, 1993.

[34] D. Somers and N. Kopell. Rapid synchronization through fast threshold modulation. *Biol. Cybern.*, **68**:393–407, 1993.

[35] D. Somers and N. Kopell. Waves and synchrony in networks of oscillators of relaxation and non- relaxation type. *Physica D*, **89**:169–183, 1995.

[36] S.H. Strogatz. *Nonlinear Dynamics and Chaos*. Addison-Wesley Publishing Company, Reading, Ma., 1994.

[37] J. Tabak, W. Senn, M.J. O'Donovan, and J. Rinzel. Comparison of two models for pattern generation based on synaptic depression. *Neurocomputing*, **26-27**:551–556, 1999.

[38] D. Terman. Chaotic spikes arising from a model for bursting in excitable membranes. *SIAM J. Appl. Math.*, **51**:1418–1450, 1991.

[39] D. Terman. The transition from bursting to continuous spiking in an excitable membrane model. *J. Nonlinear Sci.*, **2**:133–182, 1992.

[40] D. Terman, N. Kopell, and A. Bose. Dynamics of two mutually coupled inhibitory neurons. *Physica D*, **117**:241–275, 1998.

[41] D. Terman and E. Lee. Partial synchronization in a network of neural oscillators. *SIAM J. Appl. Math.*, **57**:252–293, 1997.

[42] D. Terman, J. Rubin, A.C. Yew, and C.J. Wilson. Activity patterns in a model for the subthalamopallidal network of the basal ganglia. *J. Neuroscience*, **22**:2963–2976, 2002.

[43] D. Terman and D. L. Wang. Global competition and local cooperation in a network of neural oscillators. *Physica D*, **81**:148–176, 1995.

[44] D.H. Terman, G.B. Ermentrout, and A.C. Yew. Propagating activity patterns in thalamic neuronal networks. *SIAM J. Appl. Math.*, **61**:1578–1604, 2001.

[45] X.-J. Wang and J. Rinzel. Spindle rhythmicity in the reticularis thalamic nucleus: synchronization among mutually inhibitory neurons. *Neuroscience*, **53**:899–904, 1993.

[46] X.-J. Wang and J. Rinzel. Oscillatory and bursting properties of neurons. In M.A. Arbib, editor, *The Handbook of Brain Theory and Neural Networks*, pages 686–691. The MIT Press, Cambridge, London, 1995.